International Journal of Computational Methods
Vol. 5, No. 1 (2008) 135–188

AN OVERVIEW ON SMOOTHED PARTICLE HYDRODYNAMICS

M. B. LIU*
Division of Bioengineering
Nanyang Technological University
50 Nanyang Avenue, Singapore 639798
liumb@ntu.edu.sg

G. R. LIU†
Centre for Advanced Computations in Engineering Science (ACES)
Department of Mechanical Engineering
National University of Singapore
10 Kent Ridge Crescent, Singapore 119260
mpeliugr@nus.edu.sg

Z. ZONG
School of Naval Architecture
Dalian University of Technology
Dalian 116024, China
zongzhi@dlut.edu.cn

Received 2 November 2007
Accepted 4 January 2008

This paper presents an overview on smoothed particle hydrodynamics (SPH), which is a meshfree, particle method of Lagrangian nature. In theory, the interpolation and approximations of the SPH method and the corresponding numerical errors are analyzed. The inherent particle inconsistency has been discussed in detail. It has been demonstrated that the particle inconsistency originates from the discrete particle approximation process and is the fundamental cause for poor approximation accuracy. Some particle consistency restoring approaches have been reviewed. In application, SPH modeling of general fluid dynamics and hyperdynamics with material strength have been reviewed with emphases on (1) microfluidics and microdrop dynamics, (2) coast hydrodynamics and offshore engineering, (3) environmental and geophysical flows, (4) high-explosive detonation and explosions, (5) underwater explosions, and (6) hydrodynamics with material strength including hypervelocity impact and penetration.

Keywords: Smoothed particle hydrodynamics; meshfree method; particle method; smoothing function; particle consistency.

*Corresponding author.
†SMA Fellow, Singapore-MIT Alliance.

1. Introduction

Particle methods are a general class of numerical techniques to solve real physical problem and, involve using a set of particles, each representing a volume of the simulated medium. Depending on the scale of the model, the particle may vary in size, from a small cluster of atoms or molecules to macroscopic regions in a continuum solid or fluid. Depending on the physics of the problem, each particle can be associated with a set of field variables such as mass, momentum, energy, position, charge, vorticity, etc. The particles can be fixed on the computational frame for field function approximation. This idea leads to many diversified numerical techniques such as the recently emerged meshfree methods, as reviewed in the book on meshfree methods [Liu (2003)].

The particles can also function as material points in a Lagrangian frame, and the evolution of the system is then determined by the physical conservation of mass, momentum, and energy. As such, the particle methods are strict, and can have more advantages. The classical molecular dynamics (MD) method is a typical representative of such particle methods in small (nano or micro) scales [Allen and Tildesley (1987); Xu and Liu (2003); Rapaport (2004)], in which a MD particle represents an atom or a molecule. The dissipative particle dynamics (DPD) method is another such particle method for mesoscale applications, with a DPD particle containing a small cluster of atoms or molecules [Espanol (1995); Liu *et al.* (2006b); Duong-Hong *et al.* (2007)]. For MD and DPD, the particle method gives the rigorous equations for a physical system which approximates the underlying molecular system, and is more fundamental than the common continuum equations. The force on each particle is obtained from the particle–particle interaction with neighboring particles via an interaction or force potential.

In continuum scales, there are many such particle methods of Lagrangian nature, as reviewed in some review monographs [Hockney and Eastwood (1988); Liu and Liu (2003)]. One example of this approach is the smoothed particle hydrodynamics (SPH) method [Gingold and Monaghan (1977); Lucy (1977)], which was first invented to solve astrophysical problems in three-dimensional open space. The collective movement of those particles is similar to the movement of a liquid or gas flow, and it can be modeled by the governing equations of the classical Newtonian hydrodynamics. In SPH, the state of a system is represented by a set of particles, which possess individual material properties and interact with each other within the range of a weight function (usually termed as smoothing function in SPH) [Fulk and Quinn (1996); Liu and Liu (2003); Liu *et al.* (2003c)]. The discretization of the governing equations is based on these discrete particles, and a variety of particle-based formulations have been used to calculate the local density, velocity, and acceleration of the fluid. The fluid pressure is calculated from the density using an equation of state, the particle acceleration is then calculated from the pressure gradient and the density. For low Reynolds number simulations, the effects of viscosity on the particle accelerations are also included. As a Lagrangian particle method, SPH conserves

mass exactly. In SPH, there is no explicit interface tracking — the motion of the fluid is represented by the motion of the particles, and fluid surfaces or fluid–fluid interfaces move with particles.

SPH has some special advantages over the traditional grid-based numerical methods. First, SPH is a particle method of Lagrangian nature, the algorithm is Galilean invariant. It can obtain the time history of the material particles. The advection and transport of the system can thus be calculated exactly. Second, by properly deploying particles at specific positions, with the movement of the particles, free surfaces, material interfaces, and moving boundaries which have been challenging many Eulerian methods can be obtained naturally. Another advantage is that SPH is a particle method without a grid/mesh that has commonly been used in conventional continuum numerical methods, therefore it can easily handle very large deformations, since the connectivity between particles are generated as part of the computation and can change with time. The meshfree nature of the SPH method overcomes the difficulties due to large deformations since SPH uses particles or points rather than mesh as computational frame to interpolate. These advantages make SPH attractive in modeling problems with complex physics.

The SPH method has been widely applied to modeling astrophysical phenomena, such as the simulations of binary stars and stellar collisions [Benz (1988); Monaghan (1992); Frederic and James (1999)], supernova [Hultman and Pharayn (1999); Thacker and Couchman (2001)], collapse as well as the formation of galaxies [Monaghan and Lattanzio (1991); Berczik (2000)], coalescence of black holes with neutron stars [Lee and Kluzniak (1999); Lee (2000)], single and multiple detonation of white dwarfs [Senz *et al.* (1999)], and even the evolution of the universe [Monaghan (1990)]. It has also been extended to a vast range of problems in both fluid and solid mechanics because of the strong ability to incorporate complex physics into the SPH formulations [Liu and Liu (2003)]. The applications of SPH to fluid and solid mechanics include

- multiphase flows [Monaghan and Kocharyan (1995); Colagrossi and Landrini (2003); Hu and Adams (2006b)],
- coastal hydrodynamics [Monaghan (1994); Gomez-Gesteira and Dalrymple (2004); Gotoh *et al.* (2004); Shao and Gotoh (2004); Shao (2006)],
- environmental and geophysical flows [Zhu *et al.* (1999); Zhu and Fox (2002); Tartakovsky and Meakin (2005b) (2006)],
- heat and/or mass conduction [Cleary (1998); Chen *et al.* (1999); Jeong *et al.* (2003)],
- ice and cohesive grains [Gutfraind and Savage (1998); Oger and Savage (1999)],
- microfluidics and/or microdrop dynamics [Nugent and Posch (2000); Liu and Liu (2005); Tartakovsky and Meakin (2005a)],
- high-explosive detonation and explosion [Liu *et al.* (2002, 2003d); Liu *et al.* (2003e, f, g); Liu *et al.* (2003h); Liu and Liu (2004)],

- underwater explosions and water mitigation [Swegle and Attaway (1995); Liu *et al.* (2002); Liu *et al.* (2003a); Liu *et al.* (2003f, g); Liu *et al.* (2003h)],
- elastic and/or plastic flow [Libersky and Petschek (1991); Swegle (1992); Libersky *et al.* (1993); Randles and Libersky (1996); Zhou *et al.* (2007)],
- fracture of brittle solids [Benz and Asphaug (1995)],
- metal forming and high-pressure die casting [Bonet and Kulasegaram (2000); Cleary *et al.* (2000); Cleary *et al.* (2002)],
- problems with fluid–solid interactions [Iglesias *et al.* (2004); Prakash *et al.* (2007)], and
- many other problems like blood flow [Hieber (2004); Muller (2004)], traffic flow [Rosswog and Wagner (2002)].

The early SPH algorithms were derived physically from probability theory, and statistical mechanics are extensively used as the basis for numerical estimation. They did not conserve linear and angular momentum. However, they can give reasonably good results for many astrophysical phenomena. For the simulations of fluid and solid mechanics problems, there are challenges to reproduce faithfully the partial differential equations (PDE) governing the corresponding fluid and solid dynamics. These challenges involve accuracy and stability of the numerical schemes in implementing the SPH methodology. With the development of the SPH method, and its quick applications to a wide range of problems, more attractive features have been showcased while some inherent drawbacks have been identified. Different variants or modifications have been proposed to improve the original SPH method. Gingold and Monaghan found the nonconservation of linear and angular momentum of the original SPH algorithm, and introduced an SPH algorithm that conserves both linear and angular momentum [Gingold and Monaghan (1982)]. Hu and Adams also invented an angular-momentum conservative SPH algorithm for incompressible viscous flows [Hu and Adams (2006a)]. Swegle *et al.* identified the tensile instability problem that can be important for materials with strength [Swegle *et al.* (1995)]. Morris first noted the particle inconsistency problem that can lead to poor accuracy in the SPH solution [Morris (1996)]. Over the past few years, different modifications or corrections have been tried to restore the consistency and to improve the accuracy of the SPH method. Monaghan proposed symmetrization formulations that were reported to have better effects [Monaghan (1982); Monaghan (1985); Monaghan (1992)]. Johnson and coworkers gave an axis-symmetry normalization formulation so that, for velocity fields that yield constant values of normal velocity strains, the normal velocity strains can be exactly reproduced [Johnson (1996); Johnson and Beissel (1996)]. Randles and Libersky derived a normalization formulation for the density approximation and a normalization for the divergence of the stress tensor [Randles and Libersky (1996)]. Chen *et al.* proposed a corrective smoothed particle method (CSPM) which improves the simulation accuracy both inside the problem domain and around the boundary area [Chen *et al.* (1999); Chen and Beraun (2000)]. A stress-point method was invented to improve the tensile instability and

zero energy mode problems [Dyka and Ingel (1995); Dyka *et al.* (1997); Randles and Libersky (2000); Vignjevic *et al.* (2000)]. Other notable modifications or corrections of the SPH method include the moving least-square particle hydrodynamics [Dilts (1999, 2000)], the integration kernel correction [Bonet and Kulasegaram (2000)], the reproducing kernel particle method [Chen *et al.* (1996); Liu *et al.* (1996)], the correction for stable particle method [Belytschko *et al.* (1998); Rabczuk *et al.* (2004)], and several other particle consistency restoring approaches [Liu and Liu (2003); Zhang and Batra (2004); Liu and Liu (2006)].

In this review, the interpolation scheme of the SPH method including kernel and particle approximations will be introduced first in Sec. 2, followed by error analyses on kernel and particle approximations. The concept of consistency will then be highlighted with discussions on consistency of kernel approximation (referred to as kernel consistency), and consistency of particle approximation (refereed to as particle consistency) in Sec. 3. Two particle consistency restoring approaches will be discussed thereafter. A general SPH formulation for the Navier–Stokes equations is then given for simulating general fluid dynamics in Sec. 4. In Sec. 5, some numerical aspects including smoothing length, complex boundary treatment, and time integration schemes will be discussed. More importantly, some new and notable applications of the SPH method will be reviewed in Sec. 6. Different from other review articles on SPH which may focus more on astrophysical applications, this paper emphasizes on several practical applications in fluid and solid mechanics. Section 7 gives some concluding remarks and future prospects.

2. Interpolation

The SPH method was developed for hydrodynamics problems that are basically in the form of partial differential equations (PDE) of field variables such as the density, velocity, energy, etc. An SPH formulation for a partial differential equation consists of two basic steps, the first step of integral representation (in continuous form) of a function and/or its derivatives, and the second step of summation process (in discretized from). The first step has been refereed to as *kernel approximation*, since in this procedure the approximation of a function and its derivatives are based on the evaluation of the smoothing kernel function and its derivatives. The second step has been referred to as *particle approximation*, since in this process, the estimation of the field variables on each particle are to be approximated by summing up the values of the nearest-neighbor particles.

2.1. *Kernel approximation*

The kernel approximation in the SPH methodology involves representation of a function and its derivatives by using a special function, usually termed as smoothing function. The smoothing function should satisfy some special requirements as will be discussed later, and it may also be renamed as kernel, smoothing

kernel, smoothing kernel function, or sometimes even weight function in some SPH literature [Monaghan (1992); Fulk (1994); Morris (1996); Liu *et al.* (2003c)].

The kernel approximation of a function $f(\mathbf{x})$ used in the SPH method starts from the following identity

$$f(\mathbf{x}) = \int_\Omega f(\mathbf{x}')\delta(\mathbf{x}-\mathbf{x}')d\mathbf{x}', \tag{1}$$

where f is a function of the three-dimensional position vector $\mathbf{x}$, and $\delta(\mathbf{x}-\mathbf{x}')$ is the Dirac delta function given by

$$\delta(\mathbf{x}-\mathbf{x}') = \begin{cases} 1 & \mathbf{x}=\mathbf{x}' \\ 0 & \mathbf{x}\neq\mathbf{x}'. \end{cases} \tag{2}$$

In Eq. (1), Ω is the volume of the integral that contains $\mathbf{x}$. Equation (1) implies that a function can be represented in an integral form. Since the Dirac delta function is used, the integral representation in Eq. (2) is exact and rigorous, as long as $f(\mathbf{x})$ is defined and continuous in Ω.

If the Delta function kernel $\delta(\mathbf{x}-\mathbf{x}')$ is replaced by a smoothing function $W(\mathbf{x}-\mathbf{x}', h)$, the kernel approximation of $f(\mathbf{x})$, $\langle f(\mathbf{x})\rangle$, is given by

$$\langle f(\mathbf{x})\rangle \doteq \int_\Omega f(\mathbf{x}')W(\mathbf{x}-\mathbf{x}', h)d\mathbf{x}', \tag{3}$$

where h is the smoothing length defining the influence area of the smoothing function W. Note that as long as W is not the Dirac delta function, the integral representation in Eq. (3) can only be an approximation, except for special cases. For convenience, the kernel approximation operator $\langle\ \rangle$ is usually omitted, and the sign of $\doteq$ is usually replaced with the sign of $=$. Therefore, Eq. (3) is more frequently written as

$$f(\mathbf{x}) = \int_\Omega f(\mathbf{x}')W(\mathbf{x}-\mathbf{x}', h)d\mathbf{x}'. \tag{4}$$

The approximation for the spatial derivative $\nabla\cdot f(\mathbf{x})$ is obtained simply by substituting $f(\mathbf{x})$ with $\nabla\cdot f(\mathbf{x})$ in Eq. (4), which gives

$$\nabla\cdot f(\mathbf{x}) = \int_\Omega [\nabla\cdot f(\mathbf{x}')]W(\mathbf{x}-\mathbf{x}', h)d\mathbf{x}', \tag{5}$$

where the divergence in the integral is operated with respect to the primed coordinate. Considering

$$[\nabla\cdot f(\mathbf{x}')]W(\mathbf{x}-\mathbf{x}', h) = \nabla\cdot[f(\mathbf{x}')W(\mathbf{x}-\mathbf{x}', h)] - f(\mathbf{x}')\cdot\nabla[W(\mathbf{x}-\mathbf{x}', h)], \tag{6}$$

the following equation is obtained

$$\nabla\cdot f(\mathbf{x}) = \int_\Omega \nabla\cdot[f(\mathbf{x}')W(\mathbf{x}-\mathbf{x}', h)]d\mathbf{x}' - \int_\Omega f(\mathbf{x}')\cdot\nabla[W(\mathbf{x}-\mathbf{x}', h)]d\mathbf{x}'. \tag{7}$$

The first integral on the right-hand side (RHS) of Eq. (7) can be converted using the divergence theorem into an integral over the surface S of the domain of the integration, Ω, as

$$\nabla \cdot f(\mathbf{x}) = \int_S f(\mathbf{x}')W(\mathbf{x}-\mathbf{x}',h)\cdot \vec{\mathbf{n}}\, dS - \int_\Omega f(\mathbf{x}')\cdot \nabla W(\mathbf{x}-\mathbf{x}',h)d\mathbf{x}', \tag{8}$$

where $\vec{\mathbf{n}}$ is the unit vector normal to the surface S. Since the smoothing function W is usually defined to have compact support, the value of W on the surface of the integral in Eq. (8) is zero. Therefore, the surface integral on the RHS of Eq. (8) is also zero. Hence, the kernel approximation of the derivatives can be written from Eq. (8) as

$$\nabla \cdot f(\mathbf{x}) = -\int_\Omega f(\mathbf{x}')\cdot \nabla W(\mathbf{x}-\mathbf{x}',h)d\mathbf{x}'. \tag{9}$$

Kernel approximation of higher-order derivatives can be obtained in a similar way by substituting $f(\mathbf{x})$ with the corresponding derivatives in Eq. (4), using integration by parts, divergence theorem, and some trivial transformations. Another approach is to repeatedly use Eq. (9) to obtain the kernel approximation of the higher-order derivatives, as any higher-order derivative can be regarded as the first-order derivative of its next lower-order derivative.

From the above discussions, it can be seen that the differential operation on a function is transformed into a differential operation on the smoothing function. In other words, the SPH kernel approximation of the derivative of a field function allows the spatial gradient to be determined from the values of the function and the derivatives of the smoothing function W, rather than from the derivatives of the function itself.

2.2. *Particle approximation*

Considering a problem domain Ω filled with a set of particles (usually arbitrarily distributed, see Fig. 1 for illustration in a two-dimensional domain). These particles can either be the central particles initially generated using existing mesh generation tools or concentrated particles initially generated using some kind of space discretization model such as the particle-fill model in AUTODYN [Century Dynamics Incorporated (1997)]. The state of the system is represented by these particles, each associated with field properties. These particles can be used not only for integration, interpolation, or differencing, but also for representing the material as mass particles. One may regard these particles as the mass centers of the corresponding subsections of the material. The volume of a subsection is lumped on the corresponding particle. Therefore, one particle i is associated with a fixed lumped volume ΔV_i without fixed shape. If the particle mass and density are concerned, the lumped volume can also be replaced by the corresponding mass to density ratio m_i/ρ_i. These particles can be fixed in an Eulerian frame or move in a Lagrangian frame.

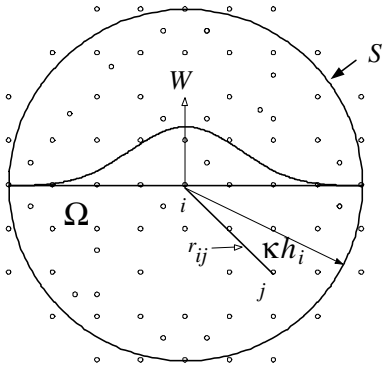

Fig. 1. SPH particle approximation in a two-dimensional problem domain Ω with a surface S. W is the smoothing function that is used to approximate the field variables at particle i through using the particles j within the support domain with a cut-off distance of κh_i.

After representing the computational domain with a finite number of particles, the continuous form of kernel approximation expressed in Eq. (4) can be written in discretized form of summation of the neighboring particles as follows

$$f(\mathbf{x}) = \sum_{j=1}^{N} \frac{m_j}{\rho_j} f(\mathbf{x}_j) W(\mathbf{x} - \mathbf{x}_j, h), \tag{10}$$

where N is the total number of particles. Due to the compactness of the smoothing function, it may also be interpreted as the total number of particles that are within the support domain which has a cut-off distance, characterized by the smoothing length, h, multiplied by a scalar constant κ. This procedure of summation on neighboring particles is referred to as particle approximation, which states that the value of a function at a particle can be approximated by using the average of those values of the function at all the particles in the support domain weighted by the smoothing function. Following the same procedure, the particle approximation of a derivative can be obtained as

$$\nabla \cdot f(\mathbf{x}) = -\sum_{j=1}^{N} \frac{m_j}{\rho_j} f(\mathbf{x}_j) \cdot \nabla W(\mathbf{x} - \mathbf{x}_j, h), \tag{11}$$

where the gradient ∇W in the above equation is taken with respect to particle j. Equation (11) states that the value of the gradient of a function at a particle can be approximated by using the summation of those values of the function at all the particles in the support domain weighted by the gradient of the smoothing function. The particle approximation in Eqs. (10) and (11) converts the continuous form of kernel approximation of a field function and its derivatives to the discretized summations based on an arbitrary set of particles. The use of particle summations to approximate the integral is, in fact, a key approximation that makes the SPH method simple without using a background mesh for numerical integration, and it is also the key factor influencing the solution accuracy of the SPH method.

3. Consistency

3.1. *Smoothing function*

Though the SPH method has been comprehensively investigated, full exploitation of the method's potential has been hampered by some unresolved numerical problems. One of the important problems is associated with the inherent SPH interpolation scheme of collocation, based only on the particles themselves. The interpolation scheme produces some other numerical issues such as numerical accuracy, consistency, and stability. Since the interpolation (kernel and particle approximation) in the SPH method involves approximating the function and its derivatives through evaluating the smoothing function and the smoothing function derivatives, the smoothing function is of utmost importance as it determines the pattern to interpolate, and defines the cut-off distance of the influencing area of a particle.

Different smoothing functions have been used in the development of the SPH method, such as the bell-shaped, quartic function by Lucy [1977], the Gaussian kernel [Gingold and Monaghan (1977)], and the cubic-spline function [Monaghan (1992)] by Monaghan and coworkers, the piecewise continuous quartic and quintic splines appeared in Morris *et al.* [1997]. The smoothing function has been studied mathematically in detail by Liu and coworkers, and they proposed a systematical way to construct a smoothing function that may meet different needs [Liu *et al.* (2003c)]. A quartic smoothing function was devised as an example to show the effectiveness of the smoothing function construction procedure. The one-piece quartic smoothing function yields a smaller second momentum, and a smoother second-order derivative, and can be more accurate and stable. Fulk did a comprehensive investigation on different smoothing function for one-dimensional cases with regular particle distribution, and he found that in general, the bell-shaped functions give better performance. However, no smoothing function is significantly better than the others [Fulk (1994); Fulk and Quinn (1996)].

A typical smoothing function should satisfy some requirements such as normalization condition, $\int W(\mathbf{x}-\mathbf{x}',h)d\mathbf{x}=1$, delta function condition, $\lim_{h\to 0} W(\mathbf{x}-\mathbf{x}',h)=\delta(x-x')$, the compactness condition, $W(\mathbf{x}-\mathbf{x}',h)=0$ for $|\mathbf{x}-\mathbf{x}'|>\kappa h$, and symmetric condition. From the compactness condition, the errors in the SPH kernel approximation of a function can be roughly estimated using Taylor series expansion of $f(\mathbf{x}')$ around $\mathbf{x}$ as follows

$$f(\mathbf{x})=\int_\Omega [f(\mathbf{x})+f'(\mathbf{x})(\mathbf{x}'-\mathbf{x})+r((\mathbf{x}'-\mathbf{x})^2)]W(\mathbf{x}-\mathbf{x}',h)d\mathbf{x}', \tag{12}$$

or

$$f(\mathbf{x})=f(\mathbf{x})\int_\Omega W(\mathbf{x}-\mathbf{x}',h)d\mathbf{x}'+f'(\mathbf{x})\int_\Omega (\mathbf{x}'-\mathbf{x})W(\mathbf{x}-\mathbf{x}',h)d\mathbf{x}'+r(h^2). \tag{13}$$

In Eqs. (12) and (13), $f(\mathbf{x})$ is differentiable, and r stands for the residual. Since W is an even function with respect to $\mathbf{x}$, $(\mathbf{x}'-\mathbf{x})W(\mathbf{x}-\mathbf{x}',h)$ should be an odd

function and $\int_\Omega (\mathbf{x}' - \mathbf{x}) W(\mathbf{x} - \mathbf{x}', h) d\mathbf{x}' = 0$. Therefore,

$$f(\mathbf{x}) = f(\mathbf{x}) \int_\Omega W(\mathbf{x} - \mathbf{x}', h) d\mathbf{x}' + r(h^2). \tag{14}$$

Equation (14) suggests that kernel approximation of a function is of second-order accuracy. However, the kernel approximation of function and/or its derivatives may not necessarily of second-order accuracy as the smoothing function may not be an even function since it is truncated when approaching the boundary region. Moreover, high-order accuracy of the kernel approximation does not necessarily mean high-order accuracy of the SPH simulations, as it is the particle approximation rather than the kernel approximation that finally determines the accuracy of the SPH simulations.

We can borrow the concept of consistency from traditional finite element methods (FEMs) [Liu and Quek (2003)]. To ensure the accuracy and convergence of an FEM approximation, the FEM shape function must satisfy a certain degree of consistency. The degree of consistency can be characterized by the order of the polynomial that can be exactly reproduced by the approximation using the shape function. In general, if an approximation can reproduce a polynomial of up to kth order exactly, the approximation is said to have kth order or C^k consistency. Similarly, it is feasible to investigate the consistency of SPH kernel and particle approximation in reproducing a polynomial by using the smoothing function.

3.2. *Kernel consistency*

For a constant (zeroth-order order polynomial) function $f(\mathbf{x}) = c$ (where c is a constant) to be exactly reproduced by the SPH kernel approximation, following Eq. (1), we have

$$f(\mathbf{x}) = \int cW(\mathbf{x} - \mathbf{x}', h) d\mathbf{x}' = c, \tag{15}$$

or

$$\int W(\mathbf{x} - \mathbf{x}', h) d\mathbf{x}' = 1. \tag{16}$$

Equation (16) is exactly the normalization condition described in Sec. 3.1.

Again, for a linear function $f(\mathbf{x}) = c_0 + c_1 \mathbf{x}$ (where c_0 and c_1 are constants) to be exactly reproduced, we have

$$f(\mathbf{x}) = \int (c_0 + c_1 \mathbf{x}') W(\mathbf{x} - \mathbf{x}', h) d\mathbf{x}' = c_0 + c_1 \mathbf{x}. \tag{17}$$

Using Eq. (15), Eq. (17) can be simplified as

$$\int \mathbf{x}' W(\mathbf{x} - \mathbf{x}', h) d\mathbf{x}' = \mathbf{x}. \tag{18}$$

Multiplying $\mathbf{x}$ on both side of Eq. (16), we have the following identity

$$\int \mathbf{x} W(\mathbf{x}-\mathbf{x}', h) d\mathbf{x}' = \mathbf{x}. \tag{19}$$

Subtracting Eq. (18) from the above identity yields

$$\int (\mathbf{x}-\mathbf{x}') W(\mathbf{x}-\mathbf{x}', h) d\mathbf{x}' = 0. \tag{20}$$

Equation (20) is the symmetric condition described in Sec. 3.1.

More generally, performing Taylor series expansion at the kernel approximation of a function $f(\mathbf{x})(= \int f(\mathbf{x}') W(\mathbf{x}-\mathbf{x}', h) d\mathbf{x}')$ in a one-dimensional space yields

$$f(\mathbf{x}) = \sum_{j=0}^{n} \frac{f^{(j)}(\mathbf{x})}{j!} \int (\mathbf{x}'-\mathbf{x})^j W(\mathbf{x}-\mathbf{x}', h) d\mathbf{x}', \tag{21}$$

where $f^{(j)}(\mathbf{x})$ is the jth derivative of function $f(\mathbf{x})$. Comparing the coefficients on both sides of Eq. (21), if an SPH approximation is to exactly reproduce a sufficiently smooth function $f(\mathbf{x})$ to nth order, the following expressions on the moments of smoothing function (M_n) can be obtained

$$\begin{aligned}
M_0 &= \int W(\mathbf{x}-\mathbf{x}', h) d\mathbf{x}' = 1 \\
M_1 &= \int (\mathbf{x}-\mathbf{x}') W(\mathbf{x}-\mathbf{x}', h) d\mathbf{x}' = 0 \\
M_2 &= \int (\mathbf{x}-\mathbf{x}')^2 W(\mathbf{x}-\mathbf{x}', h) d\mathbf{x}' = 0 \\
&\vdots \\
M_n &= \int (\mathbf{x}-\mathbf{x}')^n W(\mathbf{x}-\mathbf{x}', h) d\mathbf{x}' = 0.
\end{aligned} \tag{22}$$

Therefore, Eq. (16) (normalization condition) and (20) (symmetric condition) are actually components in Eq. (22), which describe the zeroth and first moments.

Similarly, if the derivatives of function $f(\mathbf{x})$ (up to kth order derivative) are to be exactly reproduced to nth order, another group of expressions on the derivatives of smoothing function (W^k) can be obtained

$$\begin{aligned}
W(\mathbf{x}-\mathbf{x}', h)|_S &= 0 \\
W'(\mathbf{x}-\mathbf{x}', h)|_S &= 0 \\
&\vdots \\
W^{k-1}(\mathbf{x}-\mathbf{x}', h)|_S &= 0.
\end{aligned} \tag{23}$$

For the integrations expressed in Eq. (22), the integration domain is assumed to be a full continuous support domain that is not truncated by the boundaries. Equation (22) states the requirements on the moments of a smoothing function, which are the

representations of the capability of the SPH method in reproducing polynomials. Equation (23) states that the smoothing function and its derivative should vanish at the boundaries.

Equations (22) and (23) are actually constructing conditions from which different smoothing functions can be constructed as desired [Liu *et al.* (2003c)]. In addition, these expressions are approximation accuracy indicators. If a smoothing function satisfies Eqs. (22) and (23), a function and its derivatives up to kth order can be approximated to nth order accuracy. Furthermore, the zeroth moment in Eqs. (22) states the normalization condition, and the first moment states the symmetry property of the smoothing function.

Similar to the consistency concept in the traditional FEM, if an SPH approximation can reproduce a polynomial of up to nth order exactly, the SPH approximation is said to have nth order or C^n consistency. If the consistency of an SPH kernel approximation in continuous form is termed as *kernel consistency*, the kernel consistency of an SPH kernel approximation is of nth order when the smoothing function satisfies Eq. (22). Therefore, the expressions in Eqs. (22) are also the kernel consistency conditions of the smoothing function for an SPH kernel approximation.

Note that if the SPH kernel approximations are carried out for regions truncated by boundaries, constant and linear functions cannot be reproduced exactly since Eq. (16) and (20) are not satisfied for these regions. Therefore, we can conclude that, since a conventional smoothing function satisfies the normalization and symmetric conditions, the conventional SPH method has C^1 kernel consistency for the interior regions. However, for the boundary regions, it even does not have C^0 kernel consistency.

3.3. *Particle consistency*

The kernel consistency is related to the SPH kernel approximation in continuous form. Satisfying some kernel consistency condition does not necessarily mean that the corresponding SPH particle approximations in discretized form also satisfy the discretized consistency condition. This discrepancy between the particle approximation and the kernel approximation is termed as *particle inconsistency*.

The discrete counterparts of the constant and linear consistency conditions as expressed in Eqs. (16) and (20) are

$$\sum_{j=1}^{N} W(\mathbf{x}-\mathbf{x}_j,h)\Delta v_j = 1, \tag{24}$$

and

$$\sum_{j=1}^{N} (\mathbf{x}-\mathbf{x}_j) W(\mathbf{x}-\mathbf{x}_j,h)\Delta v_j = 0. \tag{25}$$

These discretized consistency conditions are not always satisfied. One obvious and simple example is the particle approximations at the boundary particles

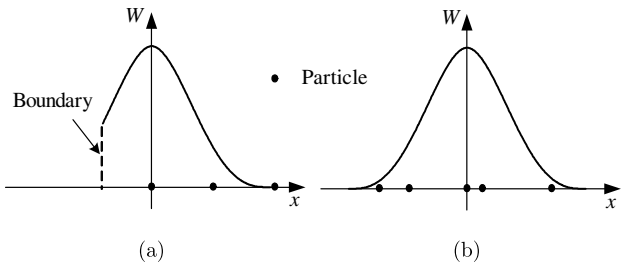

Fig. 2. SPH particle approximations in one-dimensional cases. (a) Particle approximations for a particle whose support domain is truncated by the boundary. (b) Particle approximation for a particle with irregular particle distribution in its support domain.

(Fig. 2(a)). Even for uniform particle distribution, due to the unbalanced particles contributing to the discretized summation, the left-hand side (LHS) of Eq. (24) is smaller than 1 and the LHS of Eq. (25) will not vanish, due to the truncation of the smoothing function by the boundary. For cases with irregularly distributed particles (Fig. 2(b)), it is also easy to verify that even for the interior particles whose support domains are not truncated, the constant and linear consistency conditions in the discretized form may not be exactly satisfied. Therefore, the original SPH method does not even have C^0 and C^1 consistency in the particle approximation. It is clear that the inconsistency of the particle approximation is closely related to the corresponding kernel approximation and originates from the disagreement with the corresponding kernel approximation. The particle inconsistency problem is the direct cause of the comparatively low accuracy associated with the original SPH method.

Besides the particle approximation features associated with boundary particles or irregular distributed particles, the choice of the smoothing length is also important in the particle approximation process. In a one-dimensional domain with the cubic-spline smoothing function, it is easy to verify that for uniformly distributed interior particles, the original SPH method has C^0 particle consistency if the smoothing length is taken exactly as the particle spacing ($h = \Delta x$) since Eq. (24) is satisfied. However, varying the smoothing length does not necessarily satisfy Eq. (24), and therefore influences the results obtained using the original SPH method. This is the reason that many SPH works discuss the influence of the smoothing length on the SPH approximation results.

In summary, the particle inconsistency originates from the discrepancy between the SPH kernel and particle approximations. Boundary particles, irregular distributed particles, and variable smoothing length can usually produce inconsistency in the particle approximation process.

3.4. *Particle consistency restoring approaches*

It has been shown that the original SPH method even does not have zeroth and first particle consistency. Different approaches have been used to improve the particle

inconsistency problem and therefore to improve the SPH approximation accuracy. Some of them involve reconstruction of a new smoothing function so as to satisfy the discretized consistency conditions. However, these approaches are usually not preferred for hydrodynamic simulations because the reconstructed smoothing function can be partially negative, nonsymmetric, and not monotonically decreasing. Approaches which improve the particle consistency without changing the conventional smoothing function are usually more preferable in simulating hydrodynamics.

One early approach [Monaghan (1992); Randles and Libersky (1996)] is based on the antisymmetric assumption of the derivative of a smoothing function

$$\sum_{j=1}^{N} W_{i,\alpha}\Delta v_j = 0, \tag{26}$$

where $W_{i,\alpha} = \partial W_i(\mathbf{x})/\partial \mathbf{x}^\alpha$. α is the dimension index repeated from 1 to d (d is the number of dimensions). Therefore, when approximating the derivative of a function f, the particle approximation can be rewritten as

$$f_{i,\alpha} = \sum_{j=1}^{N}(f_j - f_i)W_{i,\alpha}\Delta v_j, \tag{27}$$

or

$$f_{i,\alpha} = \sum_{j=1}^{N}(f_j + f_i)W_{i,\alpha}\Delta v_j. \tag{28}$$

It should also be noted that Eq. (26) is not necessarily valid though its corresponding continuous counterpart $\int W_{i,\alpha} d\mathbf{x} = 0$ is valid (for interior regions). This is also a manifestation of the particle inconsistency. Therefore, Eqs. (27) and (28) actually use the particle inconsistency in approximating the derivative of the smoothing function to offset or balance the particle inconsistency in approximating the derivatives of a function, with a hope to improve the accuracy of the approximations.

Randles and Libersky [1996] derived a normalization formulation for the density approximation

$$\rho_i \frac{\sum_{j=1}^{N} \rho_j W_{ij}\Delta v_j}{\sum_{j=1}^{N} W_{ij}\Delta v_j}, \tag{29}$$

and a normalization for the divergence of the stress tensor σ

$$(\nabla \cdot \sigma)_i = \frac{\sum_{j=1}^{N} (\sigma_j - \sigma_i) \otimes \nabla_i W_{ij}\Delta v_j}{\sum_{j=1}^{N} (\mathbf{x}_j - \mathbf{x}_i) \otimes \nabla_i W_{ij}\Delta v_j}, \tag{30}$$

where $\otimes$ is the tensor product. Again, Eqs. (29) and (30) also use the particle inconsistency in approximating the smoothing function and its derivatives to offset or balance the particle inconsistency in approximating a function and its derivatives, with an aim to improve the accuracy of the approximations.

Based on Taylor series expansion on the SPH approximation of a function, Chen and Beraun [2000] developed a CSPM. In one-dimensional space, the process of CSPM can be briefly discussed as follows.

Performing Taylor series expansion at a nearby point x_i, a sufficiently smooth function $f(\mathbf{x})$ can be expressed as

$$f(\mathbf{x}) = f_i + (x - x_i) f_{i,x} + \frac{(x - x_i)^2}{2!} f_{i,xx} + \cdots . \tag{31}$$

Multiplying both sides of Eq. (31) by the smoothing function W and integrating over the entire computational domain yield

$$\int f(x) W_i(x) dx = f_i \int W_i(x) dx + f_{i,x} \int (x - x_i) W_i(x) dx + \frac{f_{i,xx}}{2} \int (x - x_i)^2 W_i(x) dx + \cdots . \tag{32}$$

If the terms involving *derivatives* in this equation are neglected, a corrective kernel approximation for function $f(x)$ at particle i is obtained as

$$f_i = \frac{\int f(x) W_i(x) dx}{\int W_i(x) dx} . \tag{33}$$

For a conventional smoothing function (nonnegative and symmetric), the second term at the RHS of Eq. (32) is zero for interior region and not zero for boundary region. Therefore, the corrective kernel approximation expressed in Eq. (33) is of second-order accuracy for interior region and first-order accuracy for boundary region. Comparing Eq. (33) with Eq. (10), it is found that for the interior regions, the kernel approximations in the original SPH and CSPM are actually the same due to the satisfaction of the normalization condition (in continuous form). For the boundary regions, since the integral of the smoothing function is truncated by the boundary, the normalization condition cannot be satisfied. By retaining the nonunity denominator, CSPM restores the C^0 kernel consistency. Therefore, assuming the integration of the smoothing function in the boundary regions always to be unity as in the interior regions is the essential reason that the original SPH does not have C^0 kernel consistency.

The corresponding particle approximation for function $f(\mathbf{x})$ at particle i can be obtained by using summation over nearest particles for each term in Eq. (32) and

again neglecting the terms related to derivatives

$$f_i = \frac{\sum_{j=1}^{N} f_j \, W_{ij} \Delta v_j}{\sum_{j=1}^{N} W_{ij} \Delta v_j}. \tag{34}$$

It is to be noted that the particle approximation of the second term at the RHS of Eq. (32) is not necessarily zero even for the interior particles due to the particle inconsistency. Therefore strictly speaking, the particle approximation expressed in Eq. (34) is of first-order accuracy for both the interior and boundary particles. Only if the particles are uniformly distributed can the particle approximation of the second term at the RHS of Eq. (32) be zero. In this case, the particle approximation expressed in Eq. (34) is of second-order accuracy for the uniformly distributed interior particles.

If replacing $W_i(x)$ in Eq. (32) with $W_{i,x}$ and neglecting the *second and higher* derivatives, a corrective kernel approximation for the first derivative is generated as

$$f_{i,x} = \frac{\int [f(x) - f(x_i)] W_{i,x}(x) dx}{\int (x - x_i) W_{i,x}(x) dx}. \tag{35}$$

The particle approximations corresponding to Eq. (35) is

$$f_{i,x} = \frac{\sum_{j=1}^{N} (f_j - f_i) W_{i,x} \Delta v_j}{\sum_{j=1}^{N} (\mathbf{x}_j - \mathbf{x}_i) W_{i,x} \Delta v_j}. \tag{36}$$

Similarly, the CSPM kernel approximations for the derivatives are also of second-order accuracy (or first-order consistency) for interior regions, but first-order accuracy (or zeroth-order consistency) for boundary regions. Except for cases with uniformly distributed interior particles, the CSPM particle approximations for the derivatives are of first-order accuracy (or zeroth-order consistency) for both the interior and boundary particles.

Liu *et al.* gave another approach to restore particle inconsistency through reconstructing the smoothing function [Liu and Liu (2003)]. For a particle approximation to obtain a kth order consistency in the discrete form, the smoothing function can be written in the following form

$$\begin{aligned} W(\mathbf{x} - \mathbf{x}_j, h) &= b_0(\mathbf{x}, h) + b_1(\mathbf{x}, h) \left(\frac{\mathbf{x} - \mathbf{x}_j}{h} \right) + b_2(\mathbf{x}, h) \left(\frac{\mathbf{x} - \mathbf{x}_j}{h} \right)^2 + \cdots \\ &= \sum_{I=0}^{k} b_I(\mathbf{x}, h) \left(\frac{\mathbf{x} - \mathbf{x}_j}{h} \right)^I. \end{aligned} \tag{37}$$

By substituting the above smoothing function into Eq. (22), and after some trivial transformation, the discretized form of Eq. (22) can be written as

$$\begin{gathered}
\sum_{j=1}^{N}\left[\sum_{I=0}^{k} b_I(\mathbf{x},h)\left(\frac{\mathbf{x}-\mathbf{x}_j}{h}\right)^I\right]\Delta\mathbf{x}_j = 1\\
\sum_{j=1}^{N}\left[\left(\frac{\mathbf{x}-\mathbf{x}_j}{h}\right)\right]\left[\sum_{I=0}^{k} b_I(\mathbf{x},h)\left(\frac{\mathbf{x}-\mathbf{x}_j}{h}\right)^I\right]\Delta\mathbf{x}_j = 0\\
\vdots\\
\sum_{j=1}^{N}\left(\frac{\mathbf{x}-\mathbf{x}_j}{h}\right)^k\left[\sum_{I=0}^{k} b_I(\mathbf{x},h)\left(\frac{\mathbf{x}-\mathbf{x}_j}{h}\right)^I\right]\Delta\mathbf{x}_j = 0,
\end{gathered} \tag{38}$$

or

$$\begin{gathered}
\sum_{I=0}^{k} b_I(\mathbf{x},h)\sum_{j=1}^{N}\left(\frac{\mathbf{x}-\mathbf{x}_j}{h}\right)^I\Delta\mathbf{x}_j = 1\\
\sum_{I=0}^{k} b_I(\mathbf{x},h)\sum_{j=1}^{N}\left(\frac{\mathbf{x}-\mathbf{x}_j}{h}\right)^{I+1}\Delta\mathbf{x}_j = 0\\
\vdots\\
\sum_{I=0}^{k} b_I(\mathbf{x},h)\sum_{j=1}^{N}\left(\frac{\mathbf{x}-\mathbf{x}_j}{h}\right)^{I+k}\Delta\mathbf{x}_j = 0.
\end{gathered} \tag{39}$$

The $k+1$ coefficients $b_I(\mathbf{x},h)$ can then be determined by solving the following matrix equation

$$\underbrace{\begin{Bmatrix} m_0(\mathbf{x},h) & m_1(\mathbf{x},h) & \cdots & m_k(\mathbf{x},h)\\ m_1(\mathbf{x},h) & m_2(\mathbf{x},h) & \cdots & m_{1+k}(\mathbf{x},h)\\ \vdots & \vdots & \ddots & \vdots\\ m_k(\mathbf{x},h) & m_{k+1}(\mathbf{x},h) & \cdots & m_{k+k}(\mathbf{x},h)\end{Bmatrix}}_{M}\underbrace{\begin{Bmatrix} b_0(\mathbf{x},h)\\ b_1(\mathbf{x},h)\\ \vdots\\ b_k(\mathbf{x},h)\end{Bmatrix}}_{b} = \underbrace{\begin{Bmatrix} 1\\ 0\\ \vdots\\ 0\end{Bmatrix}}_{I}, \tag{40}$$

or

$$\mathbf{M}\mathbf{b} = \mathbf{I}, \tag{41}$$

where

$$m_k(\mathbf{x},h) = \sum_{j=1}^{N}\left(\frac{\mathbf{x}-\mathbf{x}_j}{h}\right)^k\Delta\mathbf{x}_j, \tag{42}$$

$\mathbf{M}$ is a moment matrix, $\mathbf{b}$ is a vector of coefficients, and $\mathbf{I}$ is a vector of constants.

After determining the coefficients $b_I(\mathbf{x}, h)$, the smoothing function expressed in Eq. (37) can be calculated. The procedure ensures the discretized consistency to kth order. Therefore, the particle consistency restoring process actually gives an approach to construct some kind of smoothing function for the SPH methods.

Comparing with the traditional smoothing function, which is only dependent on the particle distance and applicable for all the particles, the consistency restored smoothing function is particle-wise. It therefore depends on both the distance and position of the interacting particles. The cost-effectiveness for this approach in constructing particle-wise smoothing functions needs to be considered since it will require additional CPU time to solve the particle-wise equation (37) for all the particles. Moreover, since all particles are moving, the particle location is changing as well. Hence, the particle-wise smoothing functions need to be computed for every time step. Another problem is that, to solve Eq. (40), the moment matrix $\mathbf{M}$ is required to be nonsingular. Therefore, the particle distribution must satisfy certain conditions rather than the arbitrary distribution as in the original SPH method.

As far as the approximation is concerned, the restoring of particle consistency is an improvement on the accuracy of the particle approximation, if a method can be used to ensure a nonsingular moment matrix $\mathbf{M}$. However, it is noted that restoring the consistency in discrete form leads to some problems in simulating hydrodynamic problems. First, the resultant smoothing function is negative in some parts of the region, which can lead to unphysical representation of some field variables, such as negative density, negative energy that can lead to a breakdown of the entire computation. Second, the resultant smoothing function may not be monotonically decreasing with the increase of the particle (node) distance. Moreover, the constructed smoothing function may not be symmetric and using this nonsymmetric smoothing function violates the equal mutual interaction in physics.

Considering the disadvantages of the above-mentioned particle inconsistency restoring approach in constructing a point-wise smoothing function, Liu *et al.* devised another particle consistency restoring approach, which retains the conventional nonnegative smoothing function instead of reconstructing a new smoothing function [Liu *et al.* (2005); Liu and Liu (2006)]. The approach is also based on Taylor series expansion for a function $f(\mathbf{x})$ in multidimensional space

$$f(\mathbf{x}) = f_i + (\mathbf{x}^\alpha - \mathbf{x}_i^\alpha) f_{i,\alpha} + \frac{(\mathbf{x}^\alpha - \mathbf{x}_i^\alpha)(\mathbf{x}^\gamma - \mathbf{x}_i^\gamma)}{2!} f_{i,\alpha\gamma} + \cdots, \tag{43}$$

where γ is the dimension index repeated from 1 to d (d is the number of dimensions). Multiplying both sides of Eq. (43) with a conventional smoothing function $W_i(x)$ and its first-order derivatives $W_{i,\beta}$, neglecting the second- and high-order derivatives, we have

$$\int f(\mathbf{x}) W_i(\mathbf{x}) dx = f_i \int W_i(\mathbf{x}) d\mathbf{x} + f_{i,\alpha} \int (\mathbf{x}^\alpha - \mathbf{x}_i^\alpha) W_i(\mathbf{x}) d\mathbf{x}, \tag{44}$$

and

$$\int f(\mathbf{x})W_{i,\beta}dx = f_i \int W_{i,\beta}d\mathbf{x} + f_{i,\alpha} \int (\mathbf{x}^\alpha - \mathbf{x}_i^\alpha)W_{i,\beta}(\mathbf{x})d\mathbf{x}. \tag{45}$$

Again β is the dimension index repeated from 1 to d. The corresponding discrete forms for Eqs. (44) and (45) are

$$\sum_{j=1}^{N} f_j W_{ij}\Delta v_j = f_i \cdot \sum_{j=1}^{N} W_{ij}\Delta v_j + f_{i,\alpha} \cdot \sum_{j=1}^{N} (\mathbf{x}_j^\alpha - \mathbf{x}_i^\alpha)W_{ij}\Delta v_j, \tag{46}$$

and

$$\sum_{j=1}^{N} f_j W_{ij,\beta}\Delta v_j = f_i \cdot \sum_{j=1}^{N} W_{ij,\beta}\Delta v_j + f_{i,\alpha} \cdot \sum_{j=1}^{N} (\mathbf{x}_j^\alpha - \mathbf{x}_i^\alpha)W_{ij,\beta}\Delta v_j. \tag{47}$$

There are $d+1$ equations for $d+1$ unknowns (f_i and $f_{i,\alpha}$). Equations (46) and (47) are therefore complete for solving with respect to f_i and $f_{i,\alpha}$, and the solutions for f_i and $f_{i,\alpha}$ are

$$\begin{bmatrix} f_i \\ f_{i,\alpha} \end{bmatrix} = \begin{bmatrix} \sum_{j=1}^{N} W_{ij}\Delta v_j & \sum_{j=1}^{N} (\mathbf{x}_j^\alpha - \mathbf{x}_i^\alpha)W_{ij}\Delta v_j \\ \sum_{j=1}^{N} W_{ij,\beta}\Delta v_j & \sum_{j=1}^{N} (\mathbf{x}_j^\alpha - \mathbf{x}_i^\alpha)W_{ij,\beta}\Delta v_j \end{bmatrix}^{-1} \begin{bmatrix} \sum_{j=1}^{N} f_j W_{ij}\Delta v_j \\ \sum_{j=1}^{N} f_j W_{ij,\beta}\Delta v_j \end{bmatrix}. \tag{48}$$

In Eqs. (43), (46), and (47), the terms related to the function and the first-order derivatives are all retained, only the terms related to second- or high-order derivatives are neglected. Therefore, the resultant particle approximations for a function and its derivatives (Eq. (48)) are able to exactly reproduce a constant and a linear function (C^0 and C^1 consistency). Hence, the algorithm shown in Eq. (48) actually restores the particle consistency that conventional SPH method does not have. This particle consistency restoring approach is independent of the particle distribution (either regular or irregular), and the choices of the smoothing kernel and smoothing length. Another advantage is that this particle consistency restoring approach does not change the conventional smoothing function and should be preferable in simulating hydrodynamics.

In summary, the properties of kernel and particle consistency of the conventional SPH method, CSPM, and PCRA (particle consistency restoring approach) are described in Tables 1 and 2.

Figure 3 shows the approximation results for a linear function $f(x, y) = x + y$ using the conventional SPH method and the PCRA. The particles are uniformly distributed. It is seen that the SPH results are associated with oscillation especially near the boundary, whereas the PCRA can obtain much better results, which are in very good agreement with the analytical solution. It is worth noting that if the

Table 1. Kernel consistency of SPH, CSPM, and PCRA.

	Interior domain	Boundary area
SPH	First order	Does not have zeroth order
CSPM	First order	Zeroth order
PCRA	First order	First order

Table 2. Particle consistency of SPH, CSPM, and PCRA.

	Interior domain		Boundary area
	Regular distribution	Irregular distribution	
SPH	First order	Does not have zeroth order	Does not have zeroth order
CSPM	First order	Zeroth order	Zeroth order
PCRA	First order	First order	First order

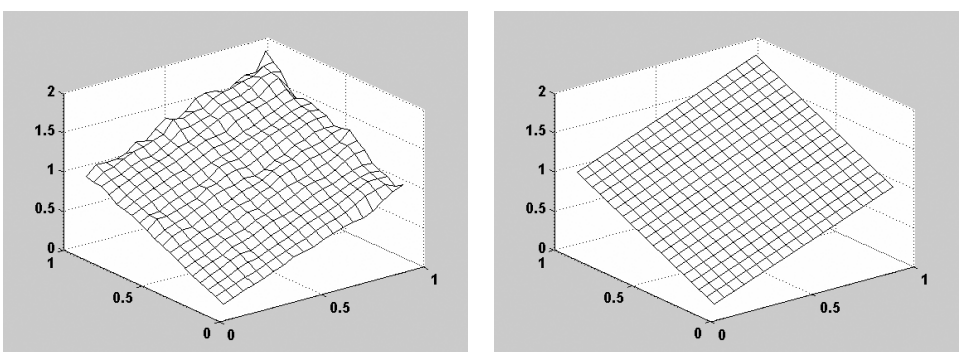

(a) (b)

Fig. 3. Approximation results for a linear function $f(x, y) = x + y$ using (a) SPH and (b) the particle consistency restoring approach in a domain of $[0, 1, 0, 1]$.

particles are randomly or irregularly distributed, PCRA can also obtain accurate results, whereas, SPH results oscillate far away from the analytical solutions. It is also worth noting that in this simple numerical test, the approximation is carried out by obtaining numerical values at current step from the existing numerical values at the particles at the previous step. There is no physical dynamics involved in these two numerical performance studies. Only the accuracy of the numerical approximations of the given function is studied using different approximation methods. It can be expected that numerical errors existing in the present approximated results can propagate to the next approximation steps and can even be magnified. However, when these methods are used to simulate a well-posed physical problem, the physics is governed by the conservation equations. If a stable numerical scheme is used, the errors present in the current step may be controlled by the governing equations.

Therefore, the errors should be more or less within some level, and will not be magnified from one step to the next step.

4. SPH Equations

Though different forms of equations can be employed to describe the fluid flows governing the corresponding physics depending on the specific circumstances, the basic governing equations of fluid dynamics are based on the fundamental physical laws of conservation of mass, momentum, and energy [Hirsch (1988); Fletcher (1991); Anderson (2002); Chung (2002)]. In general fluid dynamics, the conservation of mass, momentum, and energy in a Lagrangian frame can be expressed as

$$\frac{D\rho}{Dt} = -\rho \frac{\partial \mathbf{v}^{\beta}}{\partial \mathbf{x}^{\beta}}, \tag{49}$$

$$\frac{D\mathbf{v}^{\alpha}}{Dt} = \frac{1}{\rho} \frac{\partial \sigma^{\alpha\beta}}{\partial \mathbf{x}^{\beta}}, \tag{50}$$

and

$$\frac{De}{Dt} = \frac{\sigma^{\alpha\beta}}{\rho} \frac{\partial \mathbf{v}^{\alpha}}{\partial \mathbf{x}^{\beta}}. \tag{51}$$

These three equations are commonly referred to as continuum, momentum, and energy equations, respectively. In Eqs. (49)–(51), the Greek superscripts α and β are used to denote the coordinate directions, the summation in the equations is taken over repeated indices, and the total time derivatives are taken in the moving Lagrangian frame. The scalar density ρ, and internal energy e, the velocity component $\mathbf{v}^{\alpha}$, and the total stress tensor $\sigma^{\alpha\beta}$ are the dependent variables. The spatial coordinates $\mathbf{x}^{\alpha}$ and time t are the independent variables. The total stress tensor $\sigma^{\alpha\beta}$ is made up of two parts, one part of isotropic pressure p and the other part of viscous stress

$$\sigma^{\alpha\beta} = -p\delta^{\alpha\beta} + \tau^{\alpha\beta}. \tag{52}$$

For Newtonian fluids, the viscous shear stress should be proportional to the shear strain rate denoted by ε through the dynamic viscosity μ as

$$\tau^{\alpha\beta} = \mu\varepsilon^{\alpha\beta}, \tag{53}$$

where

$$\varepsilon^{\alpha\beta} = \frac{\partial \mathbf{v}^{\beta}}{\partial \mathbf{x}^{\alpha}} + \frac{\partial \mathbf{v}^{\alpha}}{\partial \mathbf{x}^{\beta}} - \frac{2}{3}(\nabla \cdot \mathbf{v})\delta^{\alpha\beta}. \tag{54}$$

If separating the isotropic pressure and the viscous stress, the energy equation can be rewritten as

$$\frac{De}{Dt} = -\frac{p}{\rho} \frac{\partial \mathbf{v}^{\beta}}{\partial \mathbf{x}^{\beta}} + \frac{\mu}{2\rho} \varepsilon^{\alpha\beta}\varepsilon^{\alpha\beta}. \tag{55}$$

In Eqs. (49)–(51), D/Dt is the total time derivative (or substantial derivative, material derivative, or global derivative) that is physically the time rate of change following a moving fluid elements, and it is the combination of the local derivative and the convective derivative, i.e.

$$\frac{D}{Dt} = \frac{\partial}{\partial t} + \mathbf{v}^{\alpha} \frac{\partial}{\partial \mathbf{v}^{\alpha}}, \tag{56}$$

where $\partial/\partial t$ is the local derivative that is physically the time rate of change at a fixed point; $\mathbf{v}^{\alpha}\partial/\partial \mathbf{v}^{\alpha}$ is the convective derivative that is physically the change due to the movement of the fluid element from one location to another in the flow field where the flow properties are spatially different. The total time derivative describes that the flow property of the fluid element is changing, as a fluid element sweeps passing a point in the flow.

4.1. *SPH approximation of continuum equation*

Different forms of equations of motion for the N–S equation have been developed using the SPH approximation procedure with possible transformations. In the first-ever book on SPH, the derivation of such SPH equations of motion has been described in detail with many widely used formulations given [Liu and Liu (2003)]. The advantages and disadvantages of different SPH equations of motion have also been discussed. This review article outlines some most frequently used SPH equations of motion regarding continuum, momentum, and energy equations.

Applying the SPH kernel and particle approximation concept to the continuum equation, with some trivial transformation or operation, it is possible to obtain different forms of SPH approximation of the continuum equation. One possible way is that the SPH approximation is only applied to the velocity divergence part, while the density in the RHS of the continuity equation is evaluated on the particle at which the gradient is evaluated, which is

$$\frac{D\rho_i}{Dt} = -\rho_i \sum_{j=1}^{N} \frac{m_j}{\rho_j} \mathbf{v}_j^{\beta} \cdot \frac{\partial W_{ij}}{\partial \mathbf{x}_i^{\beta}}. \tag{57}$$

Assuming Eq. (26) to be valid, it is easy to obtain another form of SPH approximation of the continuum equation as follows

$$\frac{D\rho_i}{Dt} = \rho_i \sum_{j=1}^{N} \frac{m_j}{\rho_j} \mathbf{v}_{ij}^{\beta} \cdot \frac{\partial W_{ij}}{\partial \mathbf{x}_i^{\beta}}, \tag{58}$$

by adding $\rho_i \mathbf{v}_i^{\beta} (\sum_{j=1}^{N} \frac{m_j}{\rho_j} \cdot \frac{\partial W_{ij}}{\partial \mathbf{x}_i^{\beta}})$ to Eq. (57), where $\mathbf{v}_{ij}^{\beta} = (\mathbf{v}_i^{\beta} - \mathbf{v}_j^{\beta})$. Equation (58) introduces velocity difference into the discrete particle approximation, and is usually more preferred in the SPH formulations since it accounts for the relative velocities of

particle pairs in the support domain. A direct benefit is that using the relative velocities in antisymmetrized form serves an approach to mitigate particle inconsistency, and therefore to improve approximation accuracy [Monaghan (1982); Libersky and Petschek (1991); Monaghan (1992)].

A more popular form of continuity density is to apply the following identity to place the density inside the gradient operator

$$-\rho\frac{\partial \mathbf{v}^\beta}{\partial \mathbf{x}^\beta} = -\left(\frac{\partial(\rho \mathbf{v}^\beta)}{\partial \mathbf{x}^\beta} - \mathbf{v}^\beta \cdot \frac{\partial \rho}{\partial \mathbf{x}^\beta}\right). \tag{59}$$

Similarly, if the SPH approximation is only applied to every gradient, and the velocity at the outside of the second gradient is evaluated at the particle at which the gradients are evaluated, the most frequently used continuity density equation is obtained as

$$\frac{D\rho_i}{Dt} = \sum_{j=1}^{N} m_j \mathbf{v}_{ij}^\beta \cdot \frac{\partial W_{ij}}{\partial \mathbf{x}_i^\beta}. \tag{60}$$

This equation shows clearly that the time rate of density change of a particle is closely related to the relative velocities between this particle and all the other particles in the support domain. The gradient of the smoothing function determines the contribution of these relative velocities.

If the field function is the density, Eq. (10) can be rewritten as

$$\rho_i = \sum_{j=1}^{N} m_j W_{ij}. \tag{61}$$

This is another approach to obtain density directly from the SPH summation of the mass of all particles in the support domain of a given particle, rather than from the continuum equation. Compared to the SPH formulations on density change in Eqs. (57), (58), and (60), this summation density approach conserves mass exactly, but suffers from serious boundaries deficiency due to the particle inconsistency. A frequently used way to remediate the boundaries deficiency is the following normalization form by the summation of the smoothing function itself

$$\rho_i = \frac{\sum_{j=1}^{N} m_j W_{ij}}{\sum_{j=1}^{N} \left(\frac{m_j}{\rho_j}\right) W_{ij}}. \tag{62}$$

This formulation can be directly obtained from Eq. (34). It is of first particle consistency for interior particles and zeroth particle consistency for boundary particles, therefore can have better performance in numerical accuracy than (61).

4.2. *SPH approximation of momentum equation*

The derivation of SPH formulations for particle approximation of momentum evolution is somewhat similar to the continuity density approach, and usually involves some transformations. Again, using different transformations can derive different forms of momentum approximation equations. Directly applying the SPH particle approximation concepts to the gradient on the RHS of the momentum equation (50) yields following equation

$$\frac{D\mathbf{v}_i^\alpha}{Dt} = \frac{1}{\rho_i}\sum_{j=1}^{N} m_j \frac{\sigma_j^{\alpha\beta}}{\rho_j}\frac{\partial W_{ij}}{\partial \mathbf{x}_i^\beta}. \tag{63}$$

Adding the following identity

$$\sum_{j=1}^{N} m_j \frac{\sigma_i^{\alpha\beta}}{\rho_i\rho_j}\frac{\partial W_{ij}}{\partial \mathbf{x}_i^\beta} = \frac{\sigma_i^{\alpha\beta}}{\rho_i}\left(\sum_{j=1}^{N}\frac{m_j}{\rho_j}\frac{\partial W_{ij}}{\partial \mathbf{x}_i^\beta}\right) = 0 \tag{64}$$

to Eq. (63) leads to

$$\frac{D\mathbf{v}_i^\alpha}{Dt} = \sum_{j=1}^{N} m_j \frac{\sigma_i^{\alpha\beta}+\sigma_j^{\alpha\beta}}{\rho_i\rho_j}\frac{\partial W_{ij}}{\partial \mathbf{x}_i^\beta}. \tag{65}$$

Equation (65) is a frequently used formulation to evolve momentum, and it is an early way to remediate the particle inconsistency problem.

Considering the following identity,

$$\frac{1}{\rho}\frac{\partial \sigma^{\alpha\beta}}{\partial \mathbf{x}^\beta} = \frac{\partial}{\partial \mathbf{x}^\beta}\left(\frac{\sigma^{\alpha\beta}}{\rho}\right) + \frac{\sigma^{\alpha\beta}}{\rho^2}\frac{\partial \rho}{\partial \mathbf{x}^\beta}, \tag{66}$$

and applying the SPH particle approximation to the gradients lead to

$$\frac{D\mathbf{v}_i^\alpha}{Dt} = \sum_{j=1}^{N} m_j \left(\frac{\sigma_i^{\alpha\beta}}{\rho_i^2}+\frac{\sigma_j^{\alpha\beta}}{\rho_j^2}\right)\frac{\partial W_{ij}}{\partial \mathbf{x}_i^\beta}. \tag{67}$$

Equation (67) is another very popular formulation for evolving momentum, and it can also remediate the particle inconsistency and improve approximation accuracy.

Using Eq. (52), Eqs. (65) and (67) can be rewritten, respectively, in more detail as follows

$$\frac{D\mathbf{v}_i^\alpha}{Dt} = -\sum_{j=1}^{N} m_j \frac{p_i+p_j}{\rho_i\rho_j}\frac{\partial W_{ij}}{\partial \mathbf{x}_i^\alpha} + \sum_{j=1}^{N} m_j \frac{\mu_i\varepsilon_i^{\alpha\beta}+\mu_j\varepsilon_j^{\alpha\beta}}{\rho_i\rho_j}\frac{\partial W_{ij}}{\partial \mathbf{x}_i^\beta}, \tag{68}$$

and

$$\frac{D\mathbf{v}_i^\alpha}{Dt} = -\sum_{j=1}^{N} m_j \left(\frac{p_i}{\rho_i^2} + \frac{p_j}{\rho_j^2}\right) \frac{\partial W_{ij}}{\partial \mathbf{x}_i^\alpha} + \sum_{j=1}^{N} m_j \left(\frac{\mu_i \varepsilon_i^{\alpha\beta}}{\rho_i^2} + \frac{\mu_j \varepsilon_j^{\alpha\beta}}{\rho_j^2}\right) \frac{\partial W_{ij}}{\partial \mathbf{x}_i^\alpha}. \tag{69}$$

The first parts on the RHS of Eqs. (68) and (69) are the SPH approximations for the pressure, and the second parts on the RHS of Eqs. (68) and (69) are the SPH approximations for the viscous force. It is the second part that is concerned with the physical viscosity. Considering Eq. (54), the SPH approximation of $\varepsilon^{\alpha\beta}$ for particle i can be written as

$$\varepsilon_i^{\alpha\beta} = \sum_{j=1}^{N} \frac{m_j}{\rho_j} \mathbf{v}_j^\beta \frac{\partial W_{ij}}{\partial \mathbf{x}_i^\alpha} + \sum_{j=1}^{N} \frac{m_j}{\rho_j} \mathbf{v}_j^\alpha \frac{\partial W_{ij}}{\partial \mathbf{x}_i^\beta} - \left(\frac{2}{3} \sum_{j=1}^{N} \frac{m_j}{\rho_j} \mathbf{v}_j \cdot \nabla_i W_{ij}\right) \delta^{\alpha\beta}. \tag{70}$$

Similar to the same approach in deriving SPH formulation of continuum equation, the relative velocity can be introduced to remediate the particle inconsistency. Hence, Eq. (70) can be rewritten as

$$\varepsilon_i^{\alpha\beta} = \sum_{j=1}^{N} \frac{m_j}{\rho_j} \mathbf{v}_{ji}^\beta \frac{\partial W_{ij}}{\partial \mathbf{x}_i^\alpha} + \sum_{j=1}^{N} \frac{m_j}{\rho_j} \mathbf{v}_{ji}^\alpha \frac{\partial W_{ij}}{\partial \mathbf{x}_i^\beta} - \left(\frac{2}{3} \sum_{j=1}^{N} \frac{m_j}{\rho_j} \mathbf{v}_{ji} \cdot \nabla_i W_{ij}\right) \delta^{\alpha\beta}. \tag{71}$$

The SPH approximation of $\varepsilon^{\alpha\beta}$ for particle j can be obtained in the same way. After $\varepsilon^{\alpha\beta}$ for particle i and j have been calculated, the acceleration can be calculated by Eq. (68) or (69). Note that Eq. (71) actually provides a straightforward way to model variable viscosity for different fluids.

4.3. *SPH approximation of energy equation*

For the evolution of the internal energy e in Eq. (51), the part involving strain rate can be approximated using Eq. (71). Similar to the SPH formulations for the momentum, the following SPH formulations for energy can be obtained

$$\frac{De_i}{Dt} = \frac{1}{2} \sum_{j=1}^{N} m_j \left(\frac{p_i}{\rho_i^2} + \frac{p_j}{\rho_j^2}\right) \mathbf{v}_{ij}^\beta \frac{\partial W_{ij}}{\partial \mathbf{x}_i^\beta} + \frac{\mu_i}{2\rho_i} \varepsilon_i^{\alpha\beta} \varepsilon_i^{\alpha\beta}, \tag{72}$$

$$\frac{De_i}{Dt} = \frac{1}{2} \sum_{j=1}^{N} m_j \frac{p_i + p_j}{\rho_i \rho_j} \mathbf{v}_{ij}^\beta \frac{\partial W_{ij}}{\partial \mathbf{x}_i^\beta} + \frac{\mu_i}{2\rho_i} \varepsilon_i^{\alpha\beta} \varepsilon_i^{\alpha\beta}. \tag{73}$$

Equations (72) and (73) are two commonly used formulations for approximating energy, and they can also remediate particle inconsistency due to the symmetry form. Note that if the viscosity terms in the momentum and energy equations are ignored, the SPH formulations for the Euler equations can be obtained.

5. Numerical Aspects

5.1. *Smoothing length*

Similar to those in other particle methods such as MD and DPD, the smoothing length in SPH actually defines a cut-off distance which contains the particles that can influence a given particle. However, the smoothing length can be more complicated as the cut-off distances in MD and DPD are usually constant for a given type of particle, and are directly related to the corresponding molecular diameter, while the smoothing length in SPH may vary in time, space, and even direction. The smoothing length is very important in the SPH method, which has direct influence on the efficiency of the computation and the accuracy of the solution. If the smoothing length is too small, there may not be enough particles in the support domain of dimension κh to exert forces on a given particle, which in return results in low accuracy. If the smoothing length is too large, all details of the particle or local properties may be smoothed out, and the accuracy suffers, too. The particle approximations used by the SPH method depend on having a sufficient and necessary number of particles within the support domain of κh. The computational effort or speed also depends on this particle number. In one, two, and three dimensions, the number of neighboring particles (including the particle itself) is usually set around 5, 21, and 57, respectively, if the particles are placed in a lattice with a smoothing length of 1.2 times the particle spacing, and $\kappa = 2$.

In early implementation of SPH, the global particle smoothing length was used which depended on the initial average density of the system [Gingold and Monaghan (1977); Lucy (1977)]. Later, the smoothing length was improved to solve problems where the fluid expands or contracts locally so as to maintain consistent accuracy throughout the space by assigning each particle an individual smoothing length according to the variation of the local number density of each particle [Monaghan (1992)]. For problems that are not isotropic such as shock problems, the smoothing length needs to be adapted both in space and time [Hernquist and Katz (1989); Steinmetz and Mueller (1993); Nelson (1994)].

There are many ways to dynamically evolve h so that the number of the neighboring particles remains relatively constant. A simple approach is to update the smoothing length according to the averaged density

$$h = h_0 \left(\frac{\rho_0}{\rho} \right)^{1/d}, \tag{74}$$

where h_0 and ρ_0 are the initial smoothing length and the initial density, respectively. d is the number of dimensions.

Benz [1988] suggested another method to evolve the smoothing length, which takes the time derivative of the smoothing function in terms of the continuity equation as follows

$$\frac{dh}{dt} = -\frac{1}{d} \frac{h}{\rho} \frac{d\rho}{dt}. \tag{75}$$

Liu *et al.* proposed an adaptive smoothing length model, with which only a minimum necessary number of neighbor particles will contribute to the discrete summations [Liu *et al.* (2003g)]. The model consists of a prediction step and a correction step. In the prediction step, the smoothing length is predicted using Eq. (75) with an initial smoothing length obtained from the initial density distribution. In the correction step, the number of neighboring particles within the support domain (defined by the updated smoothing length) is calculated and used to check with the initial number of neighboring particles. There is an optimal procedure to make sure that the current number of neighboring particles is not significantly far away from the initial number of neighboring particles.

More complicated models may involve smoothing length that may vary in time, space, and directions [Shapiro *et al.* (1996); Owen *et al.* (1998); Liu and Liu (2005); Liu *et al.* (2006a)]. In such models, a smoothing tensor $\mathbf{H}$ can be used to characterize the influence domain of the smoothing function

$$\mathbf{H} = \begin{pmatrix} h_{xx} & h_{yx} & h_{zx} \\ h_{xy} & h_{yy} & h_{zy} \\ h_{xz} & h_{yz} & h_{zz} \end{pmatrix}, \tag{76}$$

where $h_{yx} = h_{xy}$, $h_{zx} = h_{xz}$, and $h_{yz} = h_{zy}$. $\mathbf{H}$ is a second-order, real, and symmetric tensor. The eigenvectors of $\mathbf{H}$ are the directions along the three axes of the ellipsoid and the corresponding eigenvalues are the dimensions of the ellipsoid along each axis. It is seen that SPH can be thought of as a special case of such adaptive models, with each diagonal element of $\mathbf{H}$ equal to h while other element equal to zero. Each component in the smoothing length tensor $\mathbf{H}$ can be updated using the above-mentioned approaches for the scalar smoothing length h. Therefore, one has more freedom with ellipsoidal smoothing functions than one has with spherical smoothing functions. This tensor smoothing length model is more suitable for problems with extremely high anisotropic volume changes [Liu *et al.* (2006a)], and can greatly save computational effort for computational geometry with long channels [Liu and Liu (2005)].

5.2. *Time integration*

Similar to other explicit hydrodynamic methods, the discrete SPH approximation equations can be integrated with standard methods such as the second-order accurate Leap–Frog (LF), predictor–corrector (PC), and Runge–Kutta (RK) schemes and so on.

The Leap–Frog (LF) is the most frequently used algorithm for time integration in SPH. The advantage of the Leap–Frog algorithm is its low memory storage required in the computation and the efficiency for one force evaluation per step. The particle velocities and positions are offset by a half time-step when integrating the equations of motion. At the end of the first time-step (t_0), the change in density, energy, and

velocity are used to advance the density, energy, and velocity at half a time step, while the particle positions are advanced in a full time step as

$$\begin{aligned} t &= t_0 + \Delta t \\ \rho_i\left(t_0 + \frac{\Delta t}{2}\right) &= \rho_i(t_0) + \frac{\Delta t}{2} D\rho_i(t_0) \\ e_i\left(t_0 + \frac{\Delta t}{2}\right) &= e_i(t_0) + \frac{\Delta t}{2} De_i(t_0) \\ \mathbf{v}_i\left(t_0 + \frac{\Delta t}{2}\right) &= \mathbf{v}_i(t_0) + \frac{\Delta t}{2} D\mathbf{v}_i(t_0) \\ \mathbf{x}_i(t_0 + \Delta t) &= \mathbf{x}_i(t_0) + \Delta t \cdot \mathbf{v}_i\left(t_0 + \frac{\Delta t}{2}\right). \end{aligned} \tag{77}$$

In order to keep the calculations consistent at each subsequent time step, at the start of each subsequent time step, the density, energy, and velocity of each particle needs to be predicted at half a time step to coincide the position.

$$\begin{aligned} \rho_i(t) &= \rho_i\left(t - \frac{\Delta t}{2}\right) + \frac{\Delta t}{2} D\rho_i(t - \Delta t) \\ e_i(t) &= e_i\left(t - \frac{\Delta t}{2}\right) + \frac{\Delta t}{2} De_i(t - \Delta t) \\ \mathbf{v}_i(t) &= \mathbf{v}_i\left(t - \frac{\Delta t}{2}\right) + \frac{\Delta t}{2} D\mathbf{v}_i(t - \Delta t). \end{aligned} \tag{78}$$

At the end of the subsequent time step, the particle density, internal energy, velocity, and position are advanced in the standard Leap–Frog scheme

$$\begin{aligned} t &= t + \Delta t \\ \rho_i\left(t + \frac{\Delta t}{2}\right) &= \rho_i\left(t - \frac{\Delta t}{2}\right) + \Delta t \cdot D\rho_i(t) \\ e_i\left(t + \frac{\Delta t}{2}\right) &= e_i\left(t - \frac{\Delta t}{2}\right) + \Delta t \cdot De_i(t) \\ \mathbf{v}_i\left(t + \frac{\Delta t}{2}\right) &= \mathbf{v}_i\left(t - \frac{\Delta t}{2}\right) + \Delta t \cdot D\mathbf{v}_i(t) \\ \mathbf{x}_i(t + \Delta t) &= \mathbf{x}_i(t) + \Delta t \cdot \mathbf{v}_i\left(t + \frac{\Delta t}{2}\right). \end{aligned} \tag{79}$$

In some cases where the smoothing lengths become very small, the time step can become very small to be prohibitive. The Runge–Kutta (RK) integrator with adaptive time-step [Benz (1990); Hultman and Källander (1997)] has been shown to have an advantage during such conditions. In this case, it is possible to use adaptive time stepping, and the time step is chosen to minimize an estimate of the error in

the integration within certain tolerances. In practice, it turns out that this time step may be larger than that estimated using the Courant–Friedrichs–Levy (CFL) condition. However, it needs two force evaluations per step, and thus is computationally expensive. One of the important aspects of SPH time integration is the use of individual time-steps [Hernquist and Katz (1989)]. This treatment has advantages for problems where different time-scales naturally develop like cosmological N-body simulations.

The explicit time integration schemes are subject to the CFL condition for stability. The CFL condition states that the computational domain of dependence in a numerical simulation should include the physical domain of dependence, or the maximum speed of numerical propagation must exceed the maximum speed of physical propagation [Hirsch (1988); Anderson (2002)]. This CFL condition requires the time step to be proportional to the smallest spatial particle resolution, which in SPH applications is represented by the smallest smoothing length

$$\Delta t = \min\left(\frac{h_i}{c}\right). \tag{80}$$

The time step to be employed in an SPH application is closely related to the physical nature of the process. Monaghan [1989, 1992] gave two expressions when taking into account the viscous dissipation and the external force

$$\Delta t_{\mathrm{cv}} = \min\left(\frac{h_i}{c_i + 0.6(\alpha_\Pi c_i + \beta_\Pi \max(\phi_{ij}))}\right), \tag{81}$$

and

$$\Delta t_{\mathrm{f}} = \min\left(\frac{h_i}{f_i}\right)^{\frac{1}{2}}, \tag{82}$$

where c is the sound speed, α_Π, β_Π, and φ are constants used in the artificial viscosity [Monaghan (1992); Liu and Liu (2003)], f is the magnitude of force per unit mass (acceleration). Together with two corresponding safety coefficients, the typical time step is calculated using

$$\Delta t = \min(\lambda_1 \Delta t_{\mathrm{cv}}, \lambda_2 \Delta t_{\mathrm{f}}). \tag{83}$$

It is suggested that $\lambda_1 = 0.4$ and $\lambda_2 = 0.25$.

Morris *et al.* [1997] gave another expression for estimating time step when considering viscous diffusion

$$\Delta t = 0.125\frac{h^2}{\upsilon}, \tag{84}$$

where υ ($\upsilon = \mu/\rho$) is the kinetic viscosity.

5.3. *Solid boundary treatment and solid grains representation*

Solid boundary treatment in particle methods is always a tough task and is not as direct as that in grid-based numerical methods [Revenga *et al.* (1998); Wang

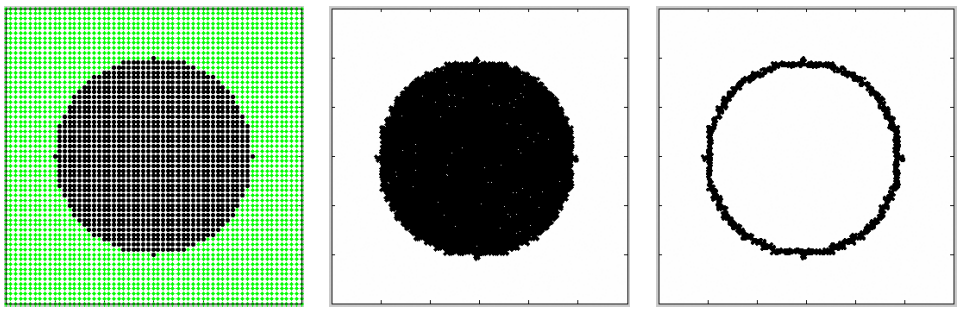

(a) (b) (c)

Fig. 4. Illustration of the treatment of solid obstacles. (a) The cells in the entire computational domain are first labeled, "0" for fluid (void) cells and "1" for solid (obstacle) cells, (b) the SPH particles in the obstacle cells are frozen. (c) Only the frozen particles that are close to the fluid cells (within one cut-off distance) are retained as boundary particles.

et al. (2006); Liu *et al.* (2007c)]. For MD and DPD, it is common to fill the solid obstacle areas with frozen particles. These fixed particles can prevent the mobile particles from penetrating the solid walls, and can interact with the mobile particles according to specific interaction models. Different complex solid matrix and solid–fluid interface physics can thus be modeled by appropriately deploying the fixed particles plus a suitable interaction model with the mobile particles.

To model geometries with complex solid matrix, the entire computational domain can be discretized using a "shadow" grid. The grid cells are labeled "0" for regions occupied by pore spaces and "1" for solid filled regions (Fig. 4a). This simple identification of fluid and solid cells can be used to represent any arbitrary complex geometry. The unit vectors normal to the solid–fluid interfaces define the local orientation of the fluid–solid interface and can be obtained by simply calculating the surface gradient from the indicator numbers ("0" for liquid regions and "1" for solid regions). At the beginning of each simulation, the particles are initialized and positioned randomly within the entire computational domain until a predefined particle number density is reached, and the system is then run to equilibrium. The particles within the solid cells (marked as "1") are then "frozen" (their positions are fixed) to represent the solid grains (Fig. 4(b)). The solid grains in obstacles can occupy a considerable fraction of the entire computational domain, and hence the number of frozen particles representing the solids can be very large. Most of the frozen particles inside the solid grains are more than one cut-off distance away from the adjacent fluid cells. These particles do not contribute to the solid–fluid interactions and consequently they have no influence on the movement of the flow particles within the fluid cells. Therefore, only the frozen particles that are within one cut-off distance from the solid-fluid interface are retained as boundary particles (Fig. 4c), and the rest of the particles further inside the solid grains are removed from the model domain.

The above approach of deploying frozen particles to represent solid grains and interact with flow particles is also applicable to SPH simulations, and it is especially effective for complex boundaries [Tartakovsky and Meakin (2005b); Liu *et al.* (2007a, b, c)]. For problems with comparatively simpler geometries, some other approaches are commonly used. These approaches may also involve particles fixed on the solid boundaries with or without equilibrium process, and may involve nonfixed boundary particles updated with the neighboring flow particles. Although fixed boundary particles are more frequently used in SPH literature, nonfixed boundary particles updated with the neighboring flow particles may produce better results [Takeda *et al.* (1994); Morris *et al.* (1997); Colagrossi and Landrini (2003); Liu and Liu (2003)].

6. Applications

SPH has been widely applied to different areas, as discussed in the introduction section. Except for the great success in astrophysical problems, the SPH method also has achieved a lot in many other engineering applications. Here, we emphasize on the following areas

- Microfluidics and microdrop dynamics,
- Coast hydrodynamics and offshore engineering,
- Environmental and geophysical flows,
- High-explosive detonation and explosions,
- Underwater explosions, and
- High strain hydrodynamics with material strength.

6.1. *Microfluidics and microdrop dynamics*

By integrating mechanical elements, sensors, actuators, and electronic components using microfabrication technology, microelectromechanical systems (MEMS) are fast in response, capable of achieving high spatial resolution, and cost-effective due to the batch micromachining techniques. Characterization of fluid flows in microfluidic devices has increasingly becoming a very important topic since the fluidic behavior in MEMS is very different from what observed in daily life. Flows in microfluidic devices usually involve small or ignorable inertial force, but dominant viscous, electrokinetic, and surface effects especially when the surface-to-volume ratio increases [Karniadakis *et al.* (2005)]. Analytical or semianalytical solutions for microfluidics are generally limited to a very few simple cases, whereas experimental studies are usually expensive. Numerical simulation of flows in microfluidic devices, as an effective alternate, has been attracting more and more researchers. However, simulation of microfluidic devices is not easy due to the involved complex features including movable boundaries (free surfaces and moving interfaces), large surface-to-volume ratio, and phenomena due to microscale physics. Numerical studies with reliable

models are needed to develop a better understanding of the temporal and spatial dynamics of multiphase flows in microfluidic devices.

On the other hand, drop formation and break-up in micro/nanoscales are fundamentally important to diverse practical engineering applications such as ink-jet printing, DNA and protein micro/nanoarraying, and fabrication of particles and capsules for controlled release of medicines. Numerical studies provide an effective tool to improve better understanding of the inherent physical dynamics of drop formation and breakup. Computational models for drop formation and breakup in micro/nanoscales must be able to handle movable boundaries such as free surfaces and moving interfaces, large density ratios, and large viscosity ratios. These requirements together with microscale phenomena and possible complex boundaries (fluid–fluid–solid contact line dynamics and fluid–fluid interface dynamics) in microfluidic devices present severe challenges to conventional Eulerian-grid-based numerical methods such as finite difference methods (FDMs), finite volume methods (FVMs) which require special algorithms to treat and track the interfaces. Algorithms based on Lagrangian-grid-based methods such as FEMs have been shown to agree quantitatively with experimental measurements, but they are only capable of modeling the dynamics of formation of a single drop or the dynamics until the occurrence of the first singularity.

A number of mesoscale methods have been developed for simulating micro and nanofluidics such as the direct-simulation Monte Carlo for rarefied gas flows [Bird (1994); Pan *et al.* (1999); Pan *et al.* (2000); Beskok and Karniadakis (2001); Pan *et al.* (2002)], and DPD for complex fluid flows [Hoogerbrugge and Koelman (1992); Groot (1997); Duong-Hong *et al.* (2007); Liu *et al.* (2007b)]. Hoover and coworkers have first noted the similarity between the particle methods of MD and SPH, and described the inherent links between them [Hoover *et al.* (1994); Hoover *et al.* (1996); Hoover and Hoover (2003)]. Espanol and his colleagues, when studying the DPD method for mesoscale applications, proposed a fluid particle dynamics model, which is actually a synthesis of DPD and smoothed particle dynamics [Espanol (1997, 1998)]. Later on, they invented a smoothed DPD for micro or mesoscale applications, by introducing a fluctuation term into the conventional SPH [Espanol and Revenga (2003)]. Liu *et al.* applied the SPH method to multiphase fluid flow in microchannels with applications in flip-chip underfill encapsulation process with both isotropic and anisotropic smoothing kernels [Liu *et al.* (2003b); Liu and Liu (2005)]. The SPH method has also been extended to multiphase fluid dynamics such as microdrop dynamics by using a van der Waals (vdW) equation of state to describe the liquid–gas coexisting system, and a special force taking account of the attraction between SPH particles [Nugent and Posch (2000); Tartakovsky and Meakin (2005a)]. It is possible to model surface tension and contact angles with SPH. Figure 5 shows the SPH simulation of the large-amplitude oscillations of a vdW fluid drop with an initial aspect ratio of 5 at eight stages. The liquid drop underwent oscillations that closely resemble the oscillations of a large ball of

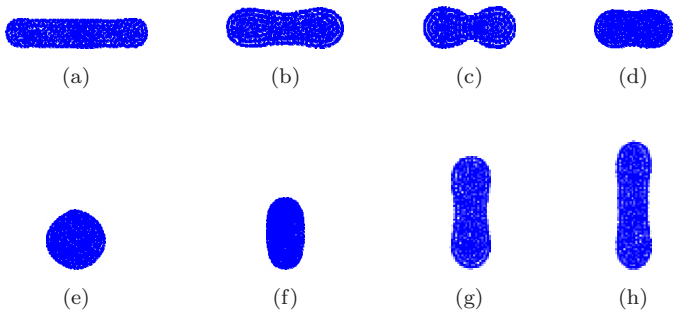

Fig. 5. SPH simulation of the large-amplitude oscillations of a vdW fluid drop with an initial aspect ratio of 5 at eight stages.

water under microgravity conditions observed experimentally in the space shuttle Columbia [Apfel *et al.* (1997)].

6.2. *Environmental and geophysical flows*

Environmental and geophysical flows are very important but they are usually difficult to simulate because of the associated multiple fluid phases and multiple physics, as well as the existence of complex geometries and arbitrarily moving interfaces. For example, fluid motion in the vadose zone is very important for groundwater recharge, fluid motion, and contaminant transport. Flow through fractures and fractured porous media can lead to exceptionally rapid movement of liquids and associated contaminants [Nativ *et al.* (1995); Scanlon *et al.* (1997); Liu *et al.* (2007c)]. The physics of fluid flows in unsaturated fractures and porous media is still poorly understood due to the complexity of multiple phase flow dynamics. Experimental studies of fluid flow in fractures and fractured porous media are limited, and in computer simulations it is usually difficult to take into account the fracture surface properties and microscopic roughness. Predictive numerical models can be divided into two general classes: volume-averaged continuum models (such as those based on Richard's equation) and discrete mechanistic models. Knowledge of the physical properties of the fluids and the geometry of the fracture apertures is required in both classes. Volume-averaged continuum models are more suitable for large-scale systems, and they usually involve the representation of fractures as porous media with porosity and permeability parameters adjusted to mimic flow within fractures. However, volume-averaged continuum models are unable to describe the details of flow dynamics in fractures, they do not reproduce the spatiotemporal complexity of multiphase fluid flow in fractures, and they often fail to predict the rapid fluid motion and contaminant transport observed in the fractured vadose zone. Small-scale studies with discrete mechanistic models are needed to develop a better understanding of the temporal and spatial dynamics of fracture flows. However, the complexity of fracture flow dynamics makes it difficult to develop

successful numerical models for fluid flows in fracture networks. A broadly applicable model must be able to simulate a variety of phenomena including film flow with free surfaces, stable rivulets, snapping rivulets, fluid fragmentation and coalescence (including coalescence/fragmentation cascades), droplet migration, and the formation of isolated single-phase islands trapped due to aperture variability.

Realistic mechanistic models for multiphase fluid flows in fracture and fractured porous media must be able to handle moving interfaces, large density ratios (e.g. ≈1000:1 for water and air), and large viscosity ratios (e.g. ≈100:1 for water and air). These requirements combined with the complex geometries of natural fractures present severe challenges to mechanistic models. Grid-based numerical methods such as FDMs, FVMs, and Eulerian FEMs require special algorithms to treat and track the interface between different phases. However, continuum grid-based numerical models usually do not take account of the detailed void and obstacle geometries, fluid–fluid interface dynamics within pores, and complex fluid–fluid–solid contact line dynamics. They rely on constitutive equations that describe the coarse-grained behavior and can, at least in principle, be derived from the results of pore scale simulations or experiments. Therefore, small-scale simulations with mechanistic models are needed to develop a better understanding of the temporal and spatial dynamics of multiphase flow through porous media. Pore-scale flows have been studied extensively using grid-based methods including FDM [Schwartz *et al.* (1993)], FVM [Huang *et al.* (2005a); Huang *et al.* (2005b)], and FEM [Snyder and Stewart (1966)]. However, due to the difficulties associated with geometrically complex boundaries, fluid–fluid–solid contact line dynamics, and fluid–fluid interface dynamics, it is difficult to apply conventional grid-based multiphase simulation methods based on computational fluid dynamics (CFD) coupled with interface tracking algorithms [Hirt and Nichols (1981); Brackbill *et al.* (1992); Unverdi and Tryggvason (1992); Sussman *et al.* (1994)] to pore-scale multiphase flow modeling.

The SPH method has been recently modified for much smaller scale, typically low Reynolds number, applications. The performance of the SPH method was demonstrated for two-dimensional single-phase flows through idealized, pore-scale porous media composed of spatially periodic square and hexagonal arrays of cylinders [Zhu *et al.* (1999); Zhu and Fox (2001)], and two-phase (miscible and immiscible) flows through pore-scale fractures and fracture junctions [Tartakovsky and Meakin (2005b,c)]. One obvious advantage of SPH over conventional grid-based methods is that SPH does not require explicit and complicated interface tracking algorithms, and thus there is no need to explicitly track the material interfaces, and processes such as fluid fragmentation and coalescence can be handled without difficulty. SPH also does not require contact angle models since contact angles can be naturally calculated from the shape of the moving particle distributions, and can vary spatially and temporally, depending on the dynamic balance of viscous, capillary, and gravitational forces. Figure 6 illustrates the snapshots of SPH simulation of multiphase fluid motion in a fractured channel network at four representative stages. Water was injected into the top entrance of the channel network using a syringe pump and

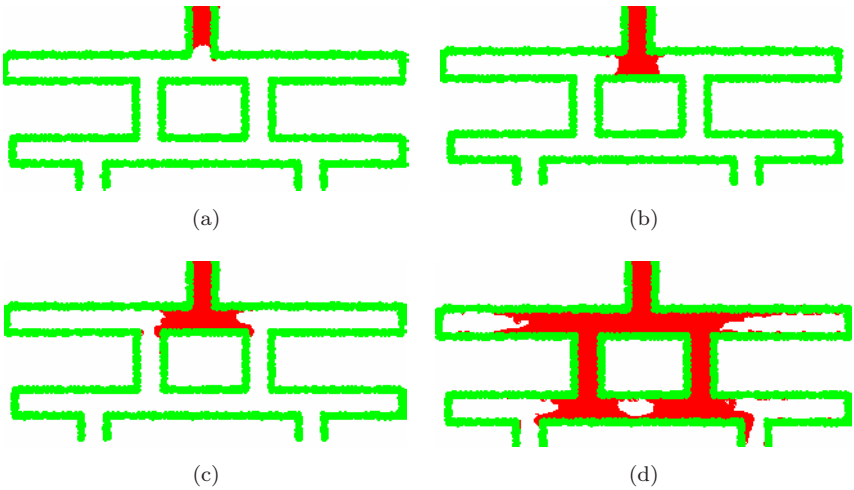

Fig. 6. Snapshots of SPH simulation of multiphase fluid motion in a fractured channel network at four representative stages.

drained out through one or two of the two channels located at the bottom of the channel network.

6.3. *Coastal hydrodynamics and offshore engineering*

Flow phenomena in coastal hydrodynamics and offshore engineering such as dam break, discharge of water from a water tank or reservoir, tsunami, flood inundation, and wave impacting on coast or structure are significantly important as they can greatly influence the nearly personnel and structures. Water waves can propagate shoreward where they undergo changes induced by the near-shore topography and increase in height. Upon reaching the shoreline, they can break into pieces, and travel inland for large distances with potential damage of property and loss of life. Experimental setups for fluid flow in coast hydrodynamics and offshore engineering are expensive and only limited to laboratory applications. Numerical simulation has thus become a great tool to predicting fluid flow in coast hydrodynamics and offshore engineering.

However, numerical simulation of fluid flow in coast hydrodynamics and offshore engineering is a formidable task as it involves not only complex geometries and free surfaces, but also fluid–solid interaction as well as other complex physics in a comparably very large scale. In many circumstances, violent fluid–structure interactions lead to air entrapment and multiphase flows, where the dynamics of the entrapped air at the impact may play a dominant role during the process and contribute to the high-pressure maxima and pressure oscillations. Though conventional grid-based methods like FDM, FVM, and FEM have been great successes in simulating fluid flow in coast hydrodynamics and offshore engineering, there is still a long way to go for practical engineering applications.

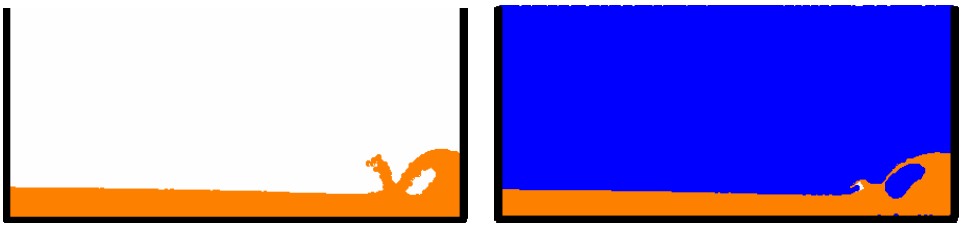

(a) (b)

Fig. 7. SPH simulation of the dam-break flow and impact against a vertical wall at (a) single phase (water only) with free surface, and (b) two phases (water and air) with moving interface.

SPH, due to its meshfree, Lagrangian and particle nature, has been attracting more and more researchers in coast hydrodynamics and offshore engineering. From the very early simulation of a simple dam break problem [Monaghan, (1994)], to the simulation of near-shore solitary wave mechanics [Lo and Shao (2002)], and to the simulation of wave impact on a tall structure [Gomez-Gesteira and Dalrymple (2004)], different SPH simulations, with possible turbulence models have emerged [Gotoh *et al.* (2004); Iglesias *et al.* (2004); Dalrymple and Rogers (2006); Shao, (2006); Shao *et al.* (2006)], and have achieved great success. Figure 7 illustrates the SPH simulation of the dam-break flow and impact against a vertical wall at (a) single phase (water only) with free surface, and (b) two phases (water and air) with moving interface. The flow pattern along the surge front, the impact of fluid against the right-hand side vertical wall, and the entrapment of air bubble in water are in good agreement with the results from other sources [Greco *et al.* (2004)].

6.4. *High-explosive detonation and explosions*

The explosion of a high-explosive (HE) charge can rapidly convert the original explosive charge into gaseous products with extremely high pressure through a chemical reaction process. The high pressure can lead to damages to nearby personnel and structures. A typical HE explosion consists of the *detonation* process through the HE at a constant detonation velocity and the later *expansion* process of the gaseous products to the surrounding medium (Fig. 8). The detonation process is accompanied by the propagation of the reactive wave that advances through the explosive with a constant velocity related to the particular type of explosive concerned. In a steady-state detonation process, the reaction rate is essentially infinite and the chemical equilibrium is attained. After the completion of the detonation, the detonation-produced explosive gas expands outwards. This gas expansion generally involves moving material interfaces if the explosive is surrounded by outside medium or free surfaces if the explosion occurs in the vacuum.

Theoretical solutions to the explosion of high-explosive are only limited to some simple cases. Experimental studies need to resort to dangerous and expensive firing trials, and sometimes certain physical phenomena related to the explosions cannot

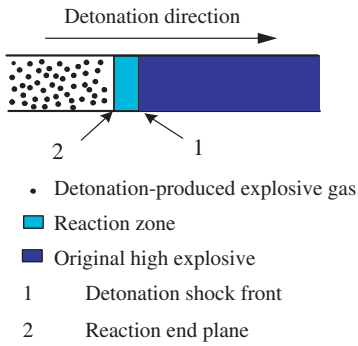

Fig. 8. Detonation of a 1D high explosive. The reaction end plane is an interface of the pressurized high-explosive charge and the explosive gas produced in the detonation process.

be scaled in a practical experimental setup. Recently, more and more analyses of high-explosive explosions are based on numerical simulations with the advancement of the computer hardware and computational techniques [Fickett and Wood (1966); Zhang (1976); Mader (1998)]. However, numerical simulations of the HE explosions are generally very difficult for the conventional grid-based numerical methods. First, during the detonation process in the explosion, a very thin reaction zone divides the domain into two inhomogeneous parts and produces large deformations. Second, in the expansion process, there are free surfaces and moving interfaces involved. Traditional Lagrangian techniques such as the FEMs are capable of capturing the history of the detonation events associated with each material. It is, however, difficult to apply practically, since the severely distorted mesh may result in very inefficient small time step, and may even lead to the breakdown of the computation. Traditional Eulerian techniques, such as the FDMs or FVMs, can well resolve the problem due to the large deformations in the global motions, but it is very difficult to analyze the details of the flow because of the lack of history and the smearing of information as the mass moves through the fixed-in-space Eulerian mesh.

Liu and coworkers have conducted a series of original work in extending the SPH method for simulating explosion phenomena including high-explosive detonation and explosion [Liu *et al.* (2001a); Liu *et al.* (2003h)], and shaped charge [Liu *et al.* (2003f)]. Since the detonation and expansion speed are extremely high, the gaseous products can be assumed to be inviscid and the explosion process is adiabatic. The Euler equations can be used to model the explosion process together with a suitable equation of state. The SPH equations of motion derived in Sec. 4 can thus be used to model high-explosive explosion phenomena, with the viscosity terms in the momentum and energy equations ignored. For the explosive gas, the standard Jones–Wilkins–Lee (JWL) [Dobratz (1981)] equation of state has been employed. These works not only show the feasibility of applying the SPH method to explosion phenomena, but also identify some important and unresolved issues.

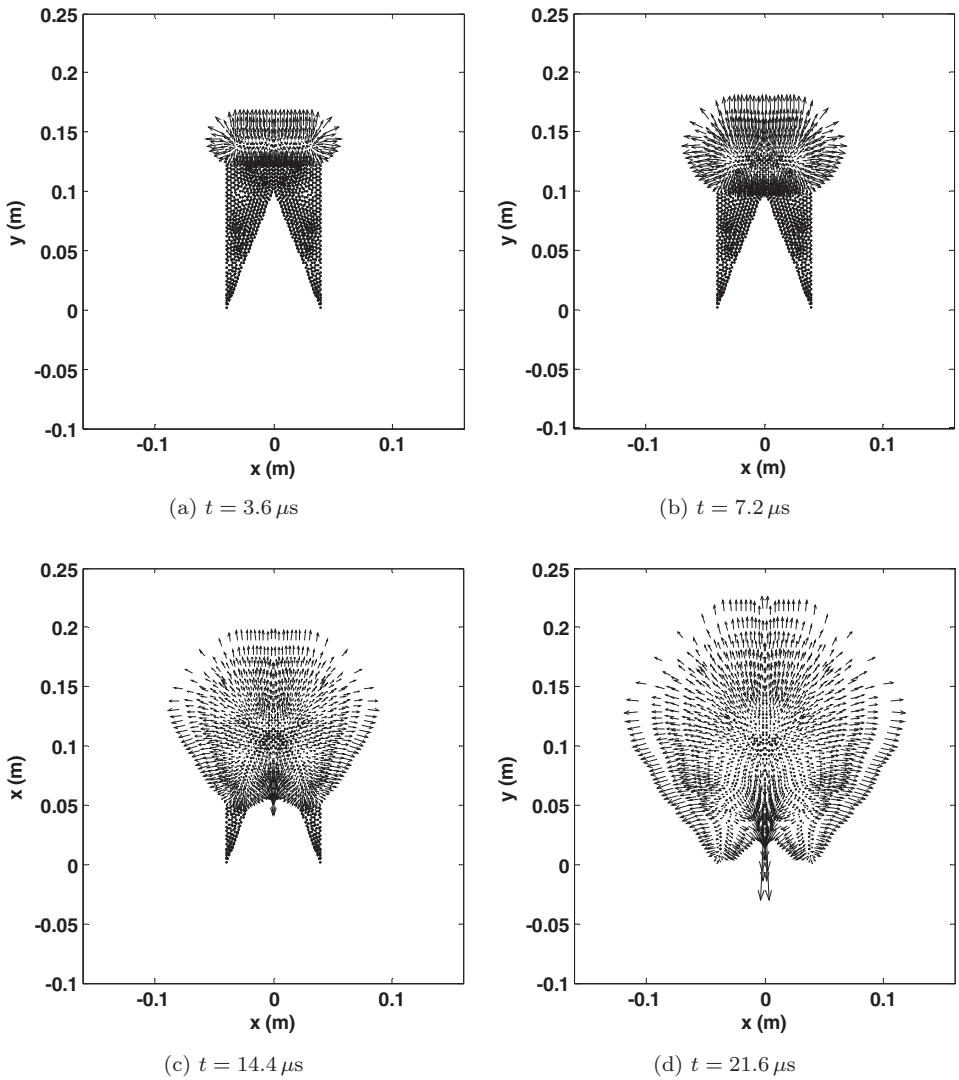

(a) $t = 3.6\,\mu$s (b) $t = 7.2\,\mu$s

(c) $t = 14.4\,\mu$s (d) $t = 21.6\,\mu$s

Fig. 9. Velocity distributions in the explosion process for a shaped charge.

Figure 9 gives an example of the SPH simulation snapshots of the explosion process of a shaped charge, with a conic cavity and a plane ignition at the upper end. The length and direction of an arrow represent the magnitude and direction of a velocity vector of a particle while the starting position of the arrow represents the location of that particle. The related physics of the shaped charge explosion process has been well captured. The detonation wave advances downwards through the explosive charge before reaching the conic cavity (a) and then the detonation wave reaches the apex of the conic cavity (b). The explosive gas later converges to the centerline and forms a gas jet traveling downwards at a very high speed

(c); and the gas jet further advances downwards with a small diverges from the centerline (d).

6.5. *Underwater explosions*

The underwater explosion (UNDEX) [Cole (1948); Bangash (1993)] produced by the detonation of a submerged high explosive poses a serious threat to the integrity of nearby structures. Issues related to the underwater explosion include (1) the detonation process of the HE charge, (2) the expansion process of the detonation-produced explosive gas into the surrounding water, and (3) the interaction of underwater shocks with the nearby structures. In the detonation process, the high explosive is converted into gaseous products at very high temperature and pressure through a violent chemical reaction, occurring with extreme rapidity and releasing a great deal of heat. The propagation of the detonation wave through an explosive is so rapid that the gaseous products directly behind the wave front are not in pressure equilibrium with the gas further behind the wave front. As the detonation wave reaches the interface between the explosive and the surrounding water, a high-pressure shock wave of step exponential type is transmitted to propagate through the water, followed by a series of bubble pulsation associated with the repeating expansion and contraction of the bubble of the explosive gas. In the entire process of the underwater explosions, some special features such as large deformations, large inhomogeneities, moving material interfaces, deformable boundaries, and free surfaces usually exist.

Underwater explosion phenomena are subject to a number of physical laws and properties, including the physical conditions at the interface of the explosive gas and the surrounding water. The surrounding water has such properties as large density that is approximately 1000 times of the air density, low compressibility, and large sound speed. Owing to the dynamic properties of the water (especially in the regions surrounding the explosive gas), the pressures are generally very high and the wave velocities are dependent on the magnitude of the pressure and the displacement of the water as it progresses. These complications for waves of finite amplitude are expressed in much more difficult mathematical statements than those which suffice to explain the propagation of small amplitude waves whose velocities are practically independent on the magnitude of the pressure.

Underwater explosion has been the subject of experimental and analytical studies since World War II. Analytical or theoretical solutions to underwater explosion problems are only limited to very simple cases. Experimental studies are fairly expensive and very dangerous due to the destructive nature of firing tests. Recently, more and more researches are focused on the numerical simulations using computers. Simulation of underwater explosion problems is a big challenge for the conventional grid-based numerical methods. On one hand, special difficulties such as large distortions, moving material interfaces, deformable boundaries, and free surfaces exist; on the other hand, the detonation process of the high explosive in the whole underwater

explosion process poses more challenges due to the complexity and larger scale of the problem.

Some early works have slightly touched the feasibility of applying the SPH method to underwater explosion related phenomena [Swegle and Attaway (1995)]. Liu and coworkers have conducted comprehensive investigations in applying the SPH method to simulating underwater explosion phenomena including confined underwater explosion [Liu *et al.* (2003g)], and water mitigations [Liu *et al.* (2002)]. They have demonstrated that the SPH simulations can capture the major physics involved in underwater explosions. Similar to the simulation of high-explosive explosion, the Euler equations and the standard Jones–Wilkins–Lee (JWL) equation of state for the explosive gaseous products have been employed. A Gruneisen form of equation of state for water has been used, which is a polynomial form either in compressed or expanded state [Chiesum and Shin (1997)].

Underwater explosions involve interfaces of explosive gas with surrounding water and water with outside air. The treatment of interface is important since the computational information is transferred through the interfaces of the media. The material interface treatment in the simulation of underwater explosion is even more complicated since the particles move more freely due to the violent interaction between the gas and water. Liu *et al.* have developed a particle-to-particle interface algorithm that was shown to be effective underwater explosion problems [Liu *et al.* (2001b)]. In the algorithm, the material interface is handled using kernel summation, which allows for interactions between particles of different materials when solving the governing conservation equation. However, it is not enough since in an underwater explosion, the violent interaction between the high-pressure explosive gas and the surrounding water usually leads to unphysical particle penetration or mixing near the interface. Hence, a penalty force is applied to particles from different materials near the interface when they are approaching and tending to penetrate each other. The penetration pe is detected (as shown in Fig. 10) if

$$pe = \frac{h_i + h_j}{2r_{ij}} \geq 1. \tag{85}$$

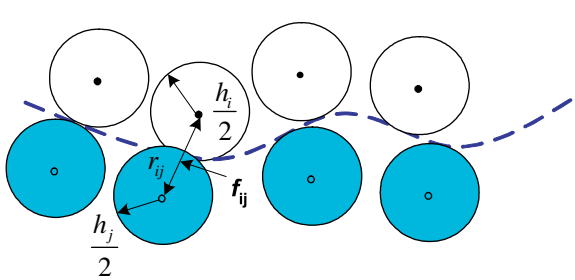

Fig. 10. Interface particles on the interface of different materials, and particle penetration.

The penalty force employed is similar to the molecular force of Lennard–Jones form and is applied pairwisely on the two approaching particles along the centerline of the two particles.

$$f_{ij} = \begin{cases} \bar{p}(pe^{n_1} - pe^{n_2})\dfrac{x_{ij}}{r_{ij}^2} & pe \geq 1 \\ 0 & pe < 1. \end{cases} \tag{86}$$

where the parameters $\bar{p}$, n_1 and n_2 are usually taken as 10^5, 6, and 4, respectively. In fact, these parameters can be adjusted to suit the needs of different problems, and the involved driven force in underwater explosions can vary in a very big range [Liu *et al.* (2001b)]. The application of the penalty force combining the summation between the interface particles has been shown to well-prevent unphysical penetration in the simulation of underwater explosion, though numerical oscillations near the vicinity of the interface can still exist.

Liu *et al.* also investigated both contact and noncontact water mitigations with different water shield thicknesses [Liu *et al.* (2002)]. Figure 11 gives an example of the SPH simulation of noncontact water mitigation. It has been identified that putting a layer of water around explosive, either in direct contact (contact water mitigation) or separated by another layer of air gap (noncontact water mitigation), generally mitigates the peak shock pressure as well as the final equilibrium gas pressure. For the contact water mitigation problems, there is an optimal water shield thickness for a given explosive charge. For the noncontact water mitigation problems, the relevant geometrical configurations of the explosive charge, air gap, and water shield must be carefully investigated. A properly designed noncontact water mitigation system can produce further mitigation effects than the contact water mitigation system. Either for the contact or noncontact water mitigation, the mitigation effect in the final equilibrium gas pressure is much more obvious than that of the peak shock pressure.

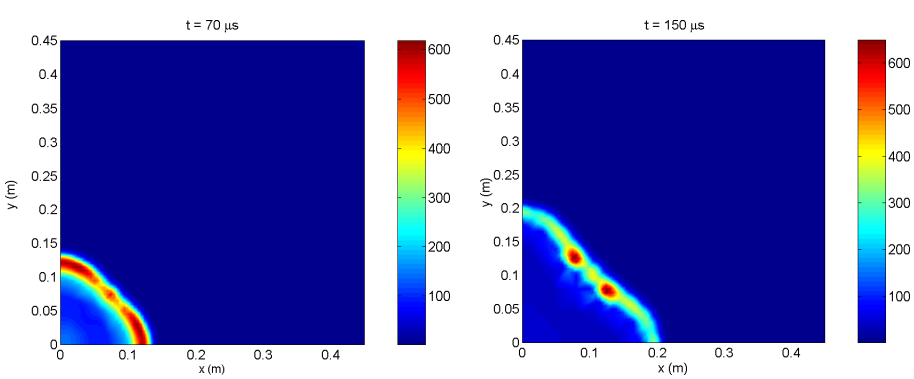

(a) Contact water mitigation (b) Non-contact water mitigation

Fig. 11. Density contour in the SPH simulations of a contact and a noncontact water mitigation. (With permission from Liu *et al.* [2002].)

6.6. *High-strain hydrodynamics with material strength*

High-strain hydrodynamics is generally characterized by the presence of shock waves, intense localized materials response, and impulsive loadings. Numerical simulation of high-strain hydrodynamics with material strength such as high-velocity impact (HVI) and penetrations is one of the formidable and attractive tasks in computational solid mechanics. Most of the wave propagation hydrocodes use traditional grid-based methods such as FDMs and FEMs to simulate high-strain hydrodynamics. Some of them are associated with advanced features which attempt to combine the best advantages of FDM and FEM. Examples include arbitrary Lagrange–Eulerian coupling and coupling Eulerian–Lagrangian. Though many successful achievements have been made using these methods, some numerical difficulties still exist. These numerical difficulties generally arise from large deformations, large inhomogeneities, and moving interfaces, free or movable boundaries [Anderson (1987); Walters and Zukas (1989); Benson (1992); Mair (1999)].

Libersky and coworkers have carried out the pioneering work of applying the SPH method to high-strain hydrodynamic problems including hypervelocity impact (HVI), fracture and fragmentation [Libersky and Petschek (1991); Libersky *et al.* (1993); Randles and Libersky (1996)]. Johnson *et al.* [1993] and Johnson and Beissel [1996] proposed a normalized smoothing function for axisymmetric problems based on the condition of uniform strain rate, and have made outstanding contributions in the application of SPH to impact problems. Attaway *et al.* have worked in coupling the SPH processor with a transient-dynamics FEM code, PRONTO, in which high-strain areas that typically tangle or break conventional finite element meshes are resolved using the SPH method [Attaway *et al.* (1998); Brown *et al.* (2000)].

Zhou and Liu have revisited the Taylor–Bar–Impact with focus on the variation of results corresponding to the different model parameters which represent varied SPH implementation in a series of three-dimensional computational simulations, and have provided informative data on appropriate SPH implementation options [Zhou *et al.* (2007)]. They also have investigated normal and oblique HVIs of a sphere on the thin plate, producing large deformation of structures. Figure 12 shows the snapshots of three-dimensional simulation of normal HVI of a sphere on the thin plate at $t = 0, 10, 15$, and $20\,\mu$s. Figure 13 shows the top (a) and three-dimensional (b) view of oblique HVI of a sphere on the thin plate at $t = 20\,\mu$s with a striking angle of 30°. They observed that for oblique HVIs of a sphere on the thin plate, the shape of the crater is no longer in circle, and the shape of the debris cloud changes with different striking angles while the ratio of the debris cloud (length over width) remains approximately 1.3.

The standard SPH method uses an isotropic smoothing kernel which is characterized by a scalar smoothing length. One of the problems associated with the standard SPH is that the isotropic kernel of SPH can be seriously mismatched to the anisotropic volume change that generally occur in many problems. To closely match the anisotropic volume changes, an anisotropic smoothing kernel which can be

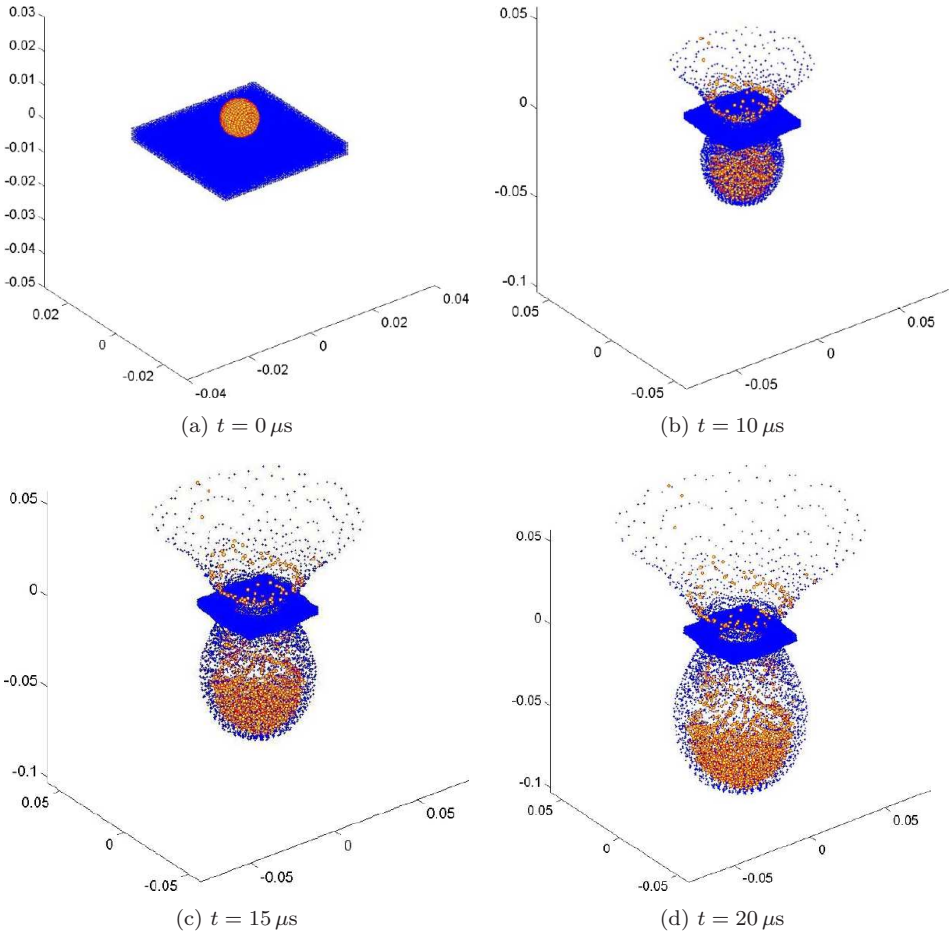

(a) $t = 0\,\mu$s (b) $t = 10\,\mu$s

(c) $t = 15\,\mu$s (d) $t = 20\,\mu$s

Fig. 12. Snapshots of three-dimensional simulation of normal hypervelocity impact of a sphere on the thin plate at $t = 0$, 10, 15, and 20 μs.

characterized by a matrix (in two-dimensional space) or tensor (in three-dimensional space) smoothing length can be efficacious. This leads to the development of the adaptive smoothed particle hydrodynamics (adaptive SPH or ASPH) in which the smoothing length can be adapted with the volume changes or other dimension-dependent features. The idea of using anisotropic kernel with SPH dates back to Bicknell and Gingold [1983]. Fulbright *et al.* also presented a three-dimensional SPH designed to model systems dominated by deformation along a preferential axis using spheroidal kernels [Fulbright *et al.* (1995)]. Later on Shapiro *et al.* systematically introduced anisotropic kernels, tensor smoothing, and shock-tracking to SPH to create ASPH [Shapiro *et al.* (1996)]. Owen *et al.* presented an alternative formulation of the ASPH algorithm for evolving anisotropic smoothing kernels [Owen *et al.* (1998)]. Except for problems with anisotropic deformations, the concept of elliptical

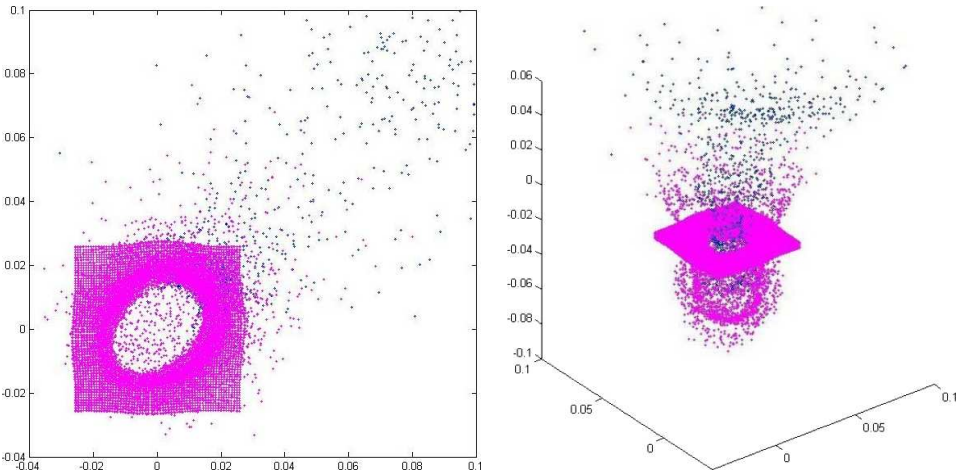

Fig. 13. Top (a) and three-dimensional (b) view of oblique hypervelocity impact of a sphere on the thin plate at $t = 20\,\mu$s with a striking angle of 30°.

kernel has also been applied to channel flows with very large length to width ratio for saving computational efforts [Liu and Liu (2005)]. The numerical results presented in the references further demonstrated that ASPH has significantly better performance than the standard SPH in terms of resolving ability for a wide range of problems.

Liu and coworkers have developed an ASPH method for high-strain Lagrangian hydrodynamics with material strength [Chin (2001); Chin *et al.* (2003); Liu *et al.* (2006a)]. In ASPH, the isotropic kernel in the standard SPH is replaced with an anisotropic kernel whose axes evolve automatically to follow the mean particle spacing as it varies in time, space, and direction around each particle. Except for the features inherited from the standard SPH, ASPH can capture dimension-dependent features such as anisotropic deformations with a more generalized elliptical or ellipsoidal influence domain. A series of comparative studies show that ASPH has better accuracy than the standard SPH when being used for high-strain hydrodynamic problems with inherent anisotropic deformations.

One example is that an Armco iron cylinder (actually a plate in two dimensions) traveling at 200 m/s impacts on a rigid surface. Figure 14 shows the steady-state particle distributions of an Armco cylinder impacting on a rigid wall using SPH and ASPH. It can be seen from the figure that there are voids formed around the center of the plate near the impact end in the SPH plots. In contrast, the particle distribution clearly shows that the particles are flattened along the direction of the impact. This obviously shows the anisotropy of the deformations. Different from the corresponding SPH plot, no void is formed around the center of the plate near the impact end. The resultant final bar height and bar width obtained using ASPH

(a) (b)

Fig. 14. Steady-state particle distribution of a cylinder impacting on a rigid wall using (a) SPH and (b) ASPH. (With permission from Liu *et al.* [2006a].)

are also in better agreement with the experimental data than the resultants obtained using SPH.

7. Concluding Remarks

As a meshfree particle method, SPH and its different modified implementations have been comprehensively investigated. The special advantages of the method have been attracting more and more practitioners with applications to various areas. This paper presents an overview on the recent developments of the SPH method in theory and applications. These recent developments can help to make full use of the potential of the SPH methodology.

One of the significant features of the SPH method is its truly meshfree nature, since the method not only uses particles as the computational frame for interpolation or differencing, but also uses the particles to carry the material properties. This truly meshfree nature is a selling point of applying the meshfree method to problems where the traditional FDM and FEM are inherently limited especially for problems with large deformations and with moving discontinuities such as cracks and shock waves.

Besides the meshfree nature, the most exciting and attractive feature of the SPH method is the harmonic combination of the Lagrangian and particle nature. Unlike the nodal points in other meshfree methods, which are only used as interpolation points, the SPH particles also carry material properties, and are allowed to move in light of the internal interactions and external forces. Functioning as interpolation points and material components, the SPH particles seem to be endowed with life. The SPH method, therefore, not only is a method for interpolation, but also provides a way to calculate the dynamic evolution of the particles. It is just the harmonic combination of the Lagrangian and particle nature in SPH that leads to various applications in different areas. Actually the particle and Lagrangian nature not

only provide a discretization tool to solve continuum mechanic problems, but also provide an appealing alternative as a physical model for noncontinuum. As can be seen from many recent literatures, except for the large deformation hydrodynamic problems that challenge the traditional grid-based methods, it is also naturally suitable for areas where the main concern of the object is a set of particles rather than a continuum (for examples, in astrophysics, solid-state physics, biochemistry, and so on), since there is no need for discretization to begin with. This has been demonstrated in the early examples of the star system formation simulation, and the recent simulation of the nanoscale movement of millions of atoms, dynamic interaction of various molecules, and so on.

To achieve a reliable solution, the computational accuracy and stability need to be taken account to incorporate into good SPH algorithms. The conventional SPH method is comparatively low in accuracy, especially for simulations with disorderly distributed particles. However, the conventional SPH method is extremely flexible, can obtain reasonable results qualitatively with ease, and can combine other complex physics readily. There are mainly three categories to improve the computational accuracy in SPH algorithms:

- Adjust or adapt the smoothing length in time, space, and/or direction [Hernquist and Katz (1989); Nelson (1994); Owen *et al.* (1998); Liu and Liu (2005)],
- Directly splitting and merging of particles [Kitsionas and Whitworth (2002)], and adaptively distributing particles [Lastiwka *et al.* (2005)],
- Particle consistency restoring approaches [Monaghan (1992); Randles and Libersky (1996); Dilts (1999); Bonet and Kulasegaram (2000); Chen and Beraun (2000); Belytschko and Xiao (2002); Liu *et al.* (2005); Liu and Liu (2006)].

Adjustment of the smoothing length can lead to results that physically describe the system evolution, whereas splitting and merging of particles can locally or globally increase the computational accuracy. However, it is necessary to establish more general and more reliable models or rules to adjust the smoothing length, to split and merge particles, and/or to adaptively distribute particles. The particle consistency restoring approaches can mathematically characterize the discretization and simulation accuracy, and is more reliable. Furthermore, the first two approaches of adjustment of smoothing length and adapting of particle number as well as position actually fall into the third approach to restore particle consistency as they are factors influencing particle consistency. Some further work needs to be done to extend these approaches to the simulation of hydrodynamic problems.

It is worth noting that SPH, as a particle method, suffers from difficulties in directly implementing solid boundary conditions. Coupling SPH with grid-based methods such as FDM or FEM can have great potential in directly implementing solid boundary conditions. Another point is that SPH shares many similarities with other particle methods such as MD and DPD, and it is natural to couple these three methods, from MD (at nano and microscales), to DPD (at mesoscales), and then to

SPH (at macroscales) for simulations with multiple scale physics. It is attractive to develop reliable models of length scale coupling for many applications to problems with multiple physics and multiple scales, such as ink-jet printing, DNA and protein micro/nanoarraying, and fabrication of particles and capsules for controlled release of medicines.

References

Allen, M. P. and Tildesley, D. J. [1987] *Computer Simulation of Liquids* (Oxford University Press).

Anderson, C. E. [1987] An overview of the theory of hydrocodes, *Int. J. Impact Eng.* **5**(1–4), 33–59.

Anderson, J. D. [2002] *Computational Fluid Dynamics: The Basics with Applications* (McGraw Hill, New York).

Apfel, R. E., Tian, Y., Jankovsky, J., Shi, T., Chen, X., Holt, R. G., Trinh, E., Croonquist, A., Thornton, K. C. and Sacco, J. A. [1997] Free oscillations and surfactant studies of superdeformed drops in microgravity, *Phys. Rev. Lett.* **78**(10), 1912–1915.

Attaway, S. W., Hendrickson, B. A., Plimpton, S. J., Gardner, D. R., Vaughan, C. T., Brown, K. H. and Heinstein, M. W. [1998] A parallel contact detection algorithm for transient solid dynamics simulations using PRONTO3D, *Comput. Mech.* **22**(2), 143–159.

Bangash, M. Y. H. [1993] *Impact and Explosion* (Blackwell Scientific Publications, Oxford).

Belytschko, T., Krongauz, Y., Dolbow, J. and Gerlach, C. [1998] On the completeness of the meshfree particle methods, *Int. J. Numer. Meth. Eng.* **43**(5), 785–819.

Belytschko, T. and Xiao, S. [2002] Stability analysis of particle methods with corrected derivatives, *Comput. Math. Appl.* **43**(3–5), 329–350.

Benson, D. J. [1992] Computational methods in Lagrangian and Eulerian hydrocodes, *Comput. Method. Appl. M.* **99**(2–3), 235–394.

Benz, W. [1988] Applications of smooth particle hydrodynamics (SPH) to astrophysical problems, *Comput. Phys. Commun.* **48**(1), 97–105.

Benz, W. [1990]. Smooth particle hydrodynamics: A review, *The Numerical Modelling of Nonlinear Stellar Pulsations, Problems and Prospects* (Kluwer Academic, Boston).

Benz, W. and Asphaug, E. [1995] Simulations of brittle solids using smooth particle hydrodynamics, *Comput. Phys. Commun.* **87**(1), 253–265.

Berczik, P. [2000] Modeling the star formation in galaxies using the chemo-dynamical SPH code, *Astrophys. Space Sci.* **271**(2), 103–126.

Beskok, A. and Karniadakis, G. E. [2001] *Microflows: Fundamentals and Simulation* (Springer, Berlin).

Bicknell, G. V. and Gingold, R. A. [1983] On tidal detonation of stars by massive black holes, *Astrophys. J.* **273**, 749–760.

Bird, G. A. [1994] *Molecular Gas Dynamics and the Direct Simulation of Gas Flows* (Oxford University Press).

Bonet, J. and Kulasegaram, S. [2000] Correction and stabilization of smooth particle hydrodynamics methods with applications in metal forming simulations, *Int. J. Numer. Meth. Eng.* **47**(6), 1189–1214.

Brackbill, J. U., Kothe, D. B. and Zemach, C. [1992] A continuum method for modeling surface tension, *J. Comput. Phys.* **100**(2), 335–354.

Brown, K., Attaway, S., Plimpton, S. and Hendrickson, B. [2000] Parallel strategies for crash and impact simulations, *Comput. Method. Appl. M.* **184**(2), 375–390.

Century Dynamics Incorporated [1997] *Autodyn Release Notes Version 3.1*, AUTODYN^{TM} Interactive Non-Linear Dynamic Analysis Software.

Chen, J. K. and Beraun, J. E. [2000] A generalized smoothed particle hydrodynamics method for nonlinear dynamic problems, *Comput. Method. Appl. M.* **190**, 225–239.

Chen, J. K., Beraun, J. E. and Carney, T. C. [1999] A corrective smoothed particle method for boundary value problems in heat conduction, *Int. J. Numer. Meth. Eng.* **46**, 231–252.

Chen, J. S., Pan, C., Wu, C. T. and Liu, W. K. [1996] Reproducing kernel particle methods for large deformation analysis of nonlinear structures, *Comput. Methods Appl. Mech. Eng.* **139**, 195–227.

Chiesum, J. E. and Shin, Y. S. [1997] Explosion gas bubbles near simple boundaries, *Shock Vib.* **4**(11), 11–25.

Chin, G. L. [2001] Smoothed particle hydrodynamics and adaptive smoothed particle hydrodynamics with strength of materials, Master Thesis, National University of Singapore.

Chin, G. L., Lam, K. Y. and Liu, G. R. [2003] Adaptive smoothed particle hydrodynamics with strength of material, Part I, *The 2nd International Conference on Structural Stability and Dynamics*, Singapore.

Chung, T. J. [2002] *Computational Fluid Dynamics* (Cambridge University Press).

Cleary, P., Ha, J., Alguine, V. and Nguyen, T. [2002] Flow modelling in casting processes, *Appl. Math. Model.* **26**(2), 171–190.

Cleary, P. W. [1998] Modelling confined multi-material heat and mass flows using SPH, *Appl. Math. Model.* **22**(12), 981–993.

Cleary, P. W., Ha, J. and Ahuja, V. [2000] High pressure die casting simulation using smoothed particle hydrodynamics, *Int. J. Cast Metal Res.* **12**(6), 335–355.

Colagrossi, A. and Landrini, M. [2003] Numerical simulation of interfacial flows by smoothed particle hydrodynamics, *J. Comput. Phys.* **191**(2), 448–475.

Cole, R. H. [1948] *Underwater Explosions* (Princeton University Press).

Dalrymple, R. A. and Rogers, B. D. [2006] Numerical modeling of water waves with the SPH method, *Coast. Eng.* **53**(2–3), 141–147.

Dilts, G. A. [1999] Moving-least-squares-particle hydrodynamics. I. Consistency and stability, *Int. J. Numer. Meth. Eng.* **44**, 1115–1155.

Dilts, G. A. [2000] Moving least square particle hydrodynamics. II. Conservation and boundaries, *Int. J. Numer. Meth. Eng.* **48**, 1503–1524.

Dobratz, B. M. [1981] *LLNL Explosive Handbook* (Lawrence Livermore National Laboratory, Livermore, CA), UCRL-52997.

Duong-Hong, D., Wang, J. S., Liu, G. R., Chen, Y. Z., Han, J. and Hadjiconstantinou, N. G. [2007] Dissipative particle dynamics simulations of electroosmotic flow in nanofluidic devices, *Microfluid. Nanofluid.* **3**, 1–7.

Dyka, C. T. and Ingel, R. P. [1995] An approach for tension instability in smoothed particle hydrodynamics (SPH), *Comput. Struct.* **57**(4), 573–580.

Dyka, C. T., Randles, P. W. and Ingel, R. P. [1997] Stress points for tension instability in SPH, *Int. J. Numer. Meth. Eng.* **40**(13), 2325–2341.

Espanol, P. [1995] Hydrodynamics from dissipative particle dynamics, *Phys. Rev. E* **52**(2), 1734–1742.

Espanol, P. [1997] Fluid particle dynamics: A synthesis of dissipative particle dynamics and smoothed particle dynamics, *Europhys. Lett.* **39**(6), 605–610.

Espanol, P. [1998] Fluid particle model, *Phys. Rev. E* **57**(3), 2930–2948.

Espanol, P. and Revenga, M. [2003] Smoothed dissipative particle dynamics, *Phys. Rev. E* **67**(2), 026705.

Fickett, W. and Wood, W. W. [1966] Flow calculations for pulsating one-dimensional detonations, *Phys. Fluids* **9**, 903–916.

Fletcher, C. A. J. [1991] *Computational Techniques for Fluid Dynamics. I. Fundamental and General Techniques* (Springer-Verlag).

Frederic, A. R. and James, C. L. [1999] Smoothed particle hydrodynamics calculations of stellar interactions, *J. Comput. Appl. Math.* **109**, 213–230.

Fulbright, M. S., Benz, W. and Davies, M. B. [1995] A method of smoothed particle hydrodynamics using spheroidal kernels, *Astrophys. J.* **440**, 254.

Fulk, D. A. [1994] A numerical analysis of smoothed particle hydrodynamics, PhD. Thesis, Air Force Institute of Technology.

Fulk, D. A. and Quinn, D. W. [1996] An analysis of 1-d smoothed particle hydrodynamics kernels, *J. Comput. Phys.* **126**(1), 165–180.

Gingold, R. A. and Monaghan, J. J. [1977] Smoothed particle hydrodynamics–theory and application to non-spherical stars, *Mon. Not. R. Astron. Soc.* **181**, 375–389.

Gingold, R. A. and Monaghan, J. J. [1982] Kernel estimates as a basis for general particle method in hydrodynamics, *J. Comput. Phys.* **46**, 429–453.

Gomez-Gesteira, M. and Dalrymple, R. A. [2004] Using a three-dimensional smoothed particle hydrodynamics method for wave impact on a tall structure, *J. Waterw. Port. C-Asce* **130**(2), 63–69.

Gotoh, H., Shao, S. D. and Memita, T. [2004] SPH-LES model for numerical investigation of wave interaction with partially immersed breakwater, *Coast. Eng. J.* **46**(1), 39–63.

Greco, M., Landrini, M. and Faltinsen, O. M. [2004] Impact flows and loads on ship-deck structures, *J. Fluids Struct.* **19**(3), 251–275.

Groot, R. D. [1997] Dissipative particle dynamics: Bridging the gap between atomistic and mesoscopic simulation, *J. Chem. Phys.* **107**(11), 4423.

Gutfraind, R. and Savage, S. B. [1998] Flow of fractured ice through wedge-shaped channels: Smoothed particle hydrodynamics and discrete-element simulations, *Mech. Mater.* **29**(1), 1–17.

Hernquist, L. and Katz, N. [1989] Treesph — a unification of SPH with the hierarchical tree method, *Astrophys. J. Suppl. S.* **70**(2), 419–446.

Hieber, S. E. [2004] Remeshed smoothed particle hydrodynamics simulation of the mechanical behavior of human organs, *Technol. Health Care* **12**(4), 305–314.

Hirsch, C. [1988] *Numerical Computation of Internal and External Flows: Fundamentals of Numerical Discretization* (Wiley, New York, NY, USA).

Hirt, C. W. and Nichols, B. D. [1981] Volume of fluid (vof) method for the dynamics of free boundaries, *J. Comput. Phys.* **39**(1), 201–225.

Hockney, R. W. and Eastwood, J. W. [1988] *Computer Simulation Using Particles* (CRC Press).

Hoogerbrugge, P. J. and Koelman, J. [1992] Simulating microscopic hydrodynamic phenomena with dissipative particle dynamics, *Europhys. Lett.* **19**, 155.

Hoover, W. G. and Hoover, C. G. [2003] Links between microscopic and macroscopic fluid mechanics, *Mol. Phys.* **101**(11), 1559–1573.

Hoover, W. G., Hoover, C. G., Kum, O., Castillo, V. M., Posch, H. A. and Hess, S. [1996] Smooth particle applied mechanics, *Comput. Methods Sci. Eng.* **2**, 6572.

Hoover, W. G., Pierce, T. G., Hoover, C. G., Shugart, J. O., Stein, C. M. and Edwards, A. L. [1994] Molecular dynamics, smoothed-particle applied mechanics, and irreversibility, *Comput. Math. Appl.* **28**(10–12), 155–174.

Hu, X. Y. and Adams, N. A. [2006a] Angular-momentum conservative smoothed particle dynamics for incompressible viscous flows, *Phys. Fluids* **18**, 101702.

Hu, X. Y. and Adams, N. A. [2006b] A multi-phase SPH method for macroscopic and mesoscopic flows, *J. Comput. Phys.* **213**(2), 844–861.

Huang, H., Meakin, P. and Liu, M. B. [2005a] Computer simulation of two-phase immiscible fluid motion in unsaturated complex fractures using a volume of fluid method, *Water Resour. Res.* **41**, W12413, doi:10.1029/2005WR004204.

Huang, H., Meakin, P., Liu, M. B. and McCreery, G. E. [2005b] Modeling of multiphase fluid motion in fracture intersections and fracture networks, *Geophys. Res. Lett.* **32**, L19402, doi:10.1029/2005GL023899.

Hultman, J. and Källander, D. [1997] Tests of a galaxy formation code, merging of particles, *Astron. Astrophys.* **324**, 534–548.

Hultman, J. and Pharayn, A. [1999] Hierarchical, dissipative formation of elliptical galaxies: Is thermal instability the key mechanism? Hydrodynamic simulations including supernova feedback multi-phase gas and metal enrichment in CDM: Structure and dynamics of elliptical galaxies, *Astron. Astrophys.* **347**, 769–798.

Iglesias, A. S., Rojas, L. P. and Rodriguez, R. Z. [2004] Simulation of anti-roll tanks and sloshing type problems with smoothed particle hydrodynamics, *Ocean Eng.* **31**(8–9), 1169–1192.

Jeong, J. H., Jhon, M. S., Halow, J. S. and Van Osdol, J. [2003] Smoothed particle hydrodynamics: Applications to heat conduction, *Comput. Phys. Commun.* **153**(1), 71–84.

Johnson, G. R. [1996] Artificial viscosity effects for SPH impact computations, *Int. J. Impact Eng.* **18**(5), 477–488.

Johnson, G. R. and Beissel, S. R. [1996] Normalized smoothing functions for SPH impact computations, *Int. J. Numer. Meth. Eng.* **39**(16), 2725–2741.

Johnson, G. R., Peterson, E. H. and Stryrk, R. A. [1993] Incorporation of an SPH option into the epic code for a wide range of high velocity impact computations, *Int. J. Impact Eng.* **14**, 385–394.

Karniadakis, G. E., Beskok, A. and Aluru, A. [2005] *Microflows and Nanoflows: Fundamentals and Simulation* (Springer).

Kitsionas, S. and Whitworth, A. P. [2002] Smoothed particle hydrodynamics with particle splitting, applied to self-gravitating collapse, *Mon. Not. R. Astron. Soc.* **330**(1), 129–136.

Lastiwka, M., Quinlan, N. and Basa, M. [2005] Adaptive particle distribution for smoothed particle hydrodynamics, *Int. J. Numer. Meth. Fl.* **47**(10–11), 1403–1409.

Lee, W. H. [2000] Newtonian hydrodynamics of the coalescence of black holes with neutron stars. III. Irrotational binaries with a stiff equation of state, *Mon. Not. R. Astron. Soc.* **318**(2), 606–624.

Lee, W. H. and Kluzniak, W. [1999] Newtonian hydrodynamics of the coalescence of black holes with neutron stars. II. Tidally locked binaries with a soft equation of state, *Mon. Not. R. Astron. Soc.* **308**(3), 780–794.

Libersky, L. D. and Petschek, A. G. [1991] Smooth particle hydrodynamics with strength of materials, *Advances in the Free-Lagrange Method Including Contributions on Adaptive Gridding and the Smooth Particle Hydrodynamics Method: Proceedings of the Next Free-Lagrange Conference* (Jackson Lake Lodge, Moran, WY, USA).

Libersky, L. D., Petschek, A. G., Carney, T. C., Hipp, J. R. and Allahdadi, F. A. [1993] High strain Lagrangian hydrodynamics: A three-dimensional SPH code for dynamic material response, *J. Comput. Phys.* **109**(1), 67–75.

Liu, G. R. [2003] *Mesh Free Methods: Moving Beyond the Finite Element Method* (CRC Press).

Liu, G. R. and Liu, M. B. [2003] *Smoothed Particle Hydrodynamics: A Meshfree Particle Method* (World Scientific Publishing Co.).

Liu, G. R. and Quek, S. S. [2003] *The Finite Element Method: A Practical Course* (Butterworth Heinemann).

Liu, M. B. and Liu, G. R. [2004] Smoothed particle hydrodynamics: Some recent developments in theory and applications, *J. Beijing Polytech. Univ.* **30**, 61–71.

Liu, M. B. and Liu, G. R. [2005] Meshfree particle simulation of micro channel flows with surface tension, *Comput. Mech.* **35**(5), 332–341.

Liu, M. B. and Liu, G. R. [2006] Restoring particle consistency in smoothed particle hydrodynamics, *Appl. Numer. Math.* **56**(1), 19–36.

Liu, M. B., Liu, G. R. and Lam, K. Y. [2001a] Simulation of the explosive detonation process by using SPH methodology, *Comput. Fluids Solid Mech.* (Elsevier Science).

Liu, M. B., Liu, G. R. and Lam, K. Y. [2002] Investigations into water mitigation using a meshless particle method, *Shock Waves* **12**(3), 181–195.

Liu, M. B., Liu, G. R. and Lam, K. Y. [2003a] Comparative study of the real and artificial detonation models in underwater explosions, *Electron. Model.* **25**(2), 113–124.

Liu, M. B., Liu, G. R. and Lam, K. Y. [2003b] Computer simulation of flip-chip underfill encapsulation process using meshfree particle method, *Int. J. Comput. Eng. Sci.* **4**(2), 405–408.

Liu, M. B., Liu, G. R. and Lam, K. Y. [2003c] Constructing smoothing functions in smoothed particle hydrodynamics with applications, *J. Comput. Appl. Math.* **155**(2), 263–284.

Liu, M. B., Liu, G. R. and Lam, K. Y. [2003d] A one-dimensional meshfree particle formulation for simulating shock waves, *Shock Waves* **13**(3), 201–211.

Liu, M. B., Liu, G. R. and Lam, K. Y. [2006a] Adaptive smoothed particle hydrodynamics for high strain hydrodynamics with material strength, *Shock Waves* **15**(1), 21–29.

Liu, M. B., Liu, G. R., Lam, K. Y. and Zong, Z. [2001b] A new technique to treat material interfaces for smoothed particle hydrodynamics, *Computational Mechanics — New Frontiers for New Millennium* (Elsevier Science), pp. 977–982.

Liu, M. B., Liu, G. R., Lam, K. Y. and Zong, Z. [2003e] Computer simulation of shaped charge detonation using meshless particle method, *Fragblast* **7**(3), 181–202.

Liu, M. B., Liu, G. R., Lam, K. Y. and Zong, Z. [2003f] Meshfree particle simulation of the detonation process for high explosives in shaped charge unlined cavity configurations, *Shock Waves* **12**(6), 509–520.

Liu, M. B., Liu, G. R., Lam, K. Y. and Zong, Z. [2003g] Smoothed particle hydrodynamics for numerical simulation of underwater explosion, *Comput. Mech.* **30**(2), 106–118.

Liu, M. B., Liu, G. R., Zong, Z. and Lam, K. Y. [2003h] Computer simulation of high explosive explosion using smoothed particle hydrodynamics methodology, *Comput. Fluids* **32**(3), 305–322.

Liu, M. B., Meakin, P. and Huang, H. [2006b] Dissipative particle dynamics with attractive and repulsive particle–particle interactions, *Phys. Fluids* **18**(1), 017101.

Liu, M. B., Meakin, P. and Huang, H. [2007a] Dissipative particle dynamics simulation of fluid motion through an unsaturated fracture and fracture junction, *J. Comput. Phys.* **222**(1), 110–130.

Liu, M. B., Meakin, P. and Huang, H. [2007b] Dissipative particle dynamics simulation of multiphase fluid flow in microchannels and microchannel networks, *Phys. Fluids* **19**(3), 033302.

Liu, M. B., Meakin, P. and Huang, H. [2007c] Dissipative particle dynamics simulation of pore-scale flow, *Water Resour. Res.* **43**, W04411, doi:10.1029/2006WR004856.

Liu, M. B., Xie, W. P. and Liu, G. R. [2005] Modeling incompressible flows using a finite particle method, *Appl. Math. Model.* **29**(12), 1252–1270.

Liu, W. K., Chen, Y., Jun, S., Chen, J. S., Belytschko, T., Pan, C., Uras, R. A. and Chang, C. T. [1996] Overview and applications of the reproducing kernel particle methods, *Arxiv. Comput. Methods Eng.* **3**(1), 3–80.

Lo, Y. M. E. and Shao, S. [2002] Simulation of near-shore solitary wave mechanics by an incompressible SPH method, *Appl. Ocean Res.* **24**(5), 275–286.

Lucy, L. B. [1977] A numerical approach to the testing of the fission hypothesis, *Astron. J.* **82**(12), 1013–1024.

Mader, C. L. [1998] *Numerical Modeling of Explosives and Propellants* (CRC Press, New York).

Mair, H. U. [1999] Review: Hydrocodes for structural response to underwater explosions, *Shock Vib.* **6**(2), 81–96.

Monaghan, J. J. [1982] Why particle methods work, *Siam J. Sci. Stat. Comp.* **3**(4), 422–433.

Monaghan, J. J. [1985] Particle methods for hydrodynamics, *Comput. Phys. Rep.* **3**, 71–124.

Monaghan, J. J. [1989] On the problem of penetration in particle methods, *J. Comput. Phys.* **82**(1), 1–15.

Monaghan, J. J. [1990] Modelling the universe, *Astron. Soc. Aust. Proc. (ISSN 0066-9997)* **8**(3), 233–237.

Monaghan, J. J. [1992] Smooth particle hydrodynamics, *Annu. Rev. Astron. Astr.* **30**, 543–574.

Monaghan, J. J. [1994] Simulating free surface flows with SPH, *J. Comput. Phys.* **110**(2), 399–406.

Monaghan, J. J. and Kocharyan, A. [1995] SPH simulation of multi-phase flow, *Comput. Phys. Commun.* **87**, 225–235.

Monaghan, J. J. and Lattanzio, J. C. [1991] A simulation of the collapse and fragmentation of cooling molecular clouds, *Astrophys. J.* **375**(1), 177–189.

Morris, J. P. [1996] Analysis of smoothed particle hydrodynamics with applications, PhD thesis, Monash University.

Morris, J. P., Fox, P. J. and Zhu, Y. [1997] Modeling low Reynolds number incompressible flows using SPH, *J. Comput. Phys.* **136**(1), 214–226.

Muller, M. [2004] Interactive blood simulation for virtual surgery based on smoothed particle hydrodynamics, *Technol. Health Care* **12**(1), 25–31.

Nativ, R., Adar, E., Dahan, O. and Geyh, M. [1995] Water recharge and solute transport through the vadose zone of fractured chalk under desert conditions, *Water Resour. Res.* **31**(2), 253–261.

Nelson, R. [1994] A conservative formulation of SPH with variable smoothing lengths, *Memorie della Societa Astronomia Italiana* **65**, 1161.

Nugent, S. and Posch, H. A. [2000] Liquid drops and surface tension with smoothed particle applied mechanics, *Phys. Rev. E* **62**(4), 4968–4975.

Oger, L. and Savage, S. B. [1999] Smoothed particle hydrodynamics for cohesive grains, *Comput. Method. Appl. M.* **180**(1), 169–183.

Owen, J. M., Villumsen, J. V., Shapiro, P. R. and Martel, H. [1998] Adaptive smoothed particle hydrodynamics: Methodology. II, *Astrophys. J. Suppl. S.* **116**(2), 155–209.

Pan, L., Ng, T. Y., Xu, D., Liu, G. R. and Lam, K. Y. [2002] Determination of temperature jump coefficient using the direct simulation Monte Carlo method, *J. Micromech. Microeng.* **12**(1), 41–52.

Pan, L. S., Liu, G. R., Khoo, B. C. and Song, B. [2000] A modified direct simulation Monte Carlo method for low-speed microflows, *J. Micromech. Microeng* **10**, 21–27.

Pan, L. S., Liu, G. R. and Lam, K. Y. [1999] Determination of slip coefficient for rarefied gas flows using direct simulation Monte Carlo, *J. Micromech. Microeng.* **9**(1), 89–96.

Prakash, M., Cleary, P. W., Ha, J., Noui-Mehidi, M. N., Blackburn, H. and Brooks, G. [2007] Simulation of suspension of solids in a liquid in a mixing tank using SPH and comparison with physical modelling experiments, *Prog. Comput. Fluid Dy.* **7**(2), 91–100.

Rabczuk, T., Belvtschko, T. and Xiao, S. P. [2004] Stable particle methods based on Lagrangian kernels, *Comput. Method. Appl. M.* **193**(12), 1035–1063.

Randles, P. W. and Libersky, L. D. [1996] Smoothed particle hydrodynamics: Some recent improvements and applications, *Comput. Method. Appl. M.* **139**(1), 375–408.

Randles, P. W. and Libersky, L. D. [2000] Normalized SPH with stress points, *Int. J. Numer. Meth. Eng.* **48**(10), 1445.

Rapaport, D. C. [2004] *The Art of Molecular Dynamics Simulation* (Cambridge University Press).

Revenga, M., Zuniga, I. and Espanol, P. [1998] Boundary models in DPD, *Int. J. Mod. Phys. C* **9**(8), 1319–1328.

Rosswog, S. and Wagner, P. [2002] Towards a macroscopic modeling of the complexity in traffic flow, *Phys. Rev. E* **65**(3), 36106.

Scanlon, B. R., Tyler, S. W. and Wierenga, P. J. [1997] Hydrologic issues in arid, unsaturated systems and implications for contaminant transport, *Rev. Geophys.* **35**(4), 461–490.

Schwartz, L. M., Martys, N., Bentz, D. P., Garboczi, E. J. and Torquato, S. [1993] Cross-property relations and permeability estimation in model porous media, *Phys. Rev. E* **48**(6), 4584–4591.

Senz, D. G., Bravo, E. and Woosley, S. E. [1999] Single and multiple detonations in white dwarfs, *Astron. Astrophys.* **349**, 177–188.

Shao, S. D. [2006] Incompressible SPH simulation of wave breaking and overtopping with turbulence modelling, *Int. J. Numer. Meth. Fl.* **50**(5), 597–621.

Shao, S. D. and Gotoh, H. [2004] Simulating coupled motion of progressive wave and floating curtain wall by SPH-LES model, *Coast. Eng. J.* **46**(2), 171–202.

Shao, S. D., Ji, C. M., Graham, D. I., Reeve, D. E., James, P. W. and Chadwick, A. J. [2006] Simulation of wave overtopping by an incompressible SPH model, *Coast. Eng.* **53**(9), 723–735.

Shapiro, P. R., Martel, H., Villumsen, J. V. and Owen, J. M. [1996] Adaptive smoothed particle hydrodynamics, with application to cosmology: Methodology, *Astrophys. J. Suppl. S.* **103**(2), 269–330.

Snyder, L. J. and Stewart, W. E. [1966] Velocity and pressure profiles for Newtonian creeping flow in regular packed beds of spheres, *AIChE, J.* **12**(1), 167–173.

Steinmetz, M. and Mueller, E. [1993] The formation of disk galaxies in a cosmological context: Populations, metallicities and metallicity gradients, *Arxiv preprint astro-ph/9312010*.

Sussman, M., Smereka, P. and Osher, S. [1994] A level set approach for computing solutions to incompressible two-phase flow, *J. Comput. Phys.* **114**(1), 146–159.

Swegle, J. W. [1992] Report at Sandia National Laboratories, August.

Swegle, J. W. and Attaway, S. W. [1995] On the feasibility of using smoothed particle hydrodynamics for underwater explosion calculations, *Comput. Mech.* **17**(3), 151–168.

Swegle, J. W., Hicks, D. L. and Attaway, S. W. [1995] Smoothed particle hydrodynamics stability analysis, *J. Comput. Phys.* **116**(1), 123–134.

Takeda, H., Miyama, S. M. and Sekiya, M. [1994] Numerical simulation of viscous flow by smoothed particle hydrodynamics, *Prog. Theor. Phys.* **92**(5), 939–960.

Tartakovsky, A. and Meakin, P. [2005a] Modeling of surface tension and contact angles with smoothed particle hydrodynamics, *Phys. Rev. E* **72**(2), 26301.

Tartakovsky, A. M. and Meakin, P. [2005b] Simulation of unsaturated flow in complex fractures using smoothed particle hydrodynamics, *Vadose Zone J.* **4**(3), 848–855.

Tartakovsky, A. M. and Meakin, P. [2005c] A smoothed particle hydrodynamics model for miscible flow in three-dimensional fractures and the two-dimensional Rayleigh Taylor instability, *J. Comput. Phys.* **207**(2), 610–624.

Tartakovsky, A. M. and Meakin, P. [2006] Pore scale modeling of immiscible and miscible fluid flows using smoothed particle hydrodynamics, *Adv. Water Resour.* **29**(10), 1464–1478.

Thacker, R. J. and Couchman, H. M. P. [2001] Star formation, supernova feedback, and the angular momentum problem in numerical cold dark matter cosmogony: Halfway there, *Astrophys. J.* **555**(1), L17–L20.

Unverdi, S. O. and Tryggvason, G. [1992] A front-tracking method for viscous, incompressible, multi-fluid flows, *J. Comput. Phys.* **100**(1), 25–37.

Vignjevic, R., Campbell, J. and Libersky, L. [2000] A treatment of zero-energy modes in the smoothed particle hydrodynamics method, *Comput. Method. Appl. M.* **184**(1), 67–85.

Walters, W. P. and Zukas, J. A. [1989] *Fundamentals of Shaped Charges* (Wiley).

Wang, L., Ge, W. and Li, J. [2006] A new wall boundary condition in particle methods, *Comput. Phys. Commun.* **174**(5), 386–390.

Xu, Y. G. and Liu, G. R. [2003] Fitting interatomatic potential using molecular dyanmics simulation and intergeneration projection genetic algorithm, *J. Micromech. Microeng.* **13**, 254–260.

Zhang, G. M. and Batra, R. C. [2004] Modified smoothed particle hydrodynamics method and its application to transient problems, *Comput. Mech.* **34**(2), 137–146.

Zhang, S. Z. [1976] *Detonation and its Applications* (Press of National Defense Industry, Beijing).

Zhou, C. E., Liu, G. R. and Lou, K. Y. [2007] Three-dimensional penetration simulation using smoothed particle hydrodynamics, *Int. J. Comput. Methods* **4**(4), 671–691.

Zhu, Y. and Fox, P. J. [2001] Smoothed particle hydrodynamics model for diffusion through porous media, *Transport Porous Med.* **43**(3), 441–471.

Zhu, Y. and Fox, P. J. [2002] Simulation of pore-scale dispersion in periodic porous media using smoothed particle hydrodynamics, *J. Comput. Phys.* **182**(2), 622–645.

Zhu, Y., Fox, P. J. and Morris, J. P. [1999] A pore-scale numerical model for flow through porous media, *Int. J. Numer. Anal. Met.* **23**(9), 881–904.